Genitourinary System

17

Ania Z. Kielar, Nicola Schieda,
and Matthew D. McInnes

Contents

Abbreviations

CECT	Contrast-enhanced CT
CSI	Chemical shift imaging
CT	Computed tomography
GU	Genitourinary
HU	Hounsfield unit
MRI	Magnetic resonance imaging
NECT	Non-enhanced CT
ROI	Region of interest

17.1 Introduction

All imaging modalities have a role in genitourinary (GU) imaging, including radiographs, fluoroscopy, ultrasound imaging, computed tomography (CT), magnetic resonance imaging (MRI), and nuclear medicine imaging. Each has

A.Z. Kielar, MD, FRCPC (✉) • N. Schieda, MD, FRCPC
M.D. McInnes, MD, FRCPC
Department of Radiology, The Ottawa Hospital,
University of Ottawa, Ottawa, ON, Canada
e-mail: akielar@toh.on.ca; nschieda@toh.on.ca;
mmcinnes@toh.on.ca

W.C.G. Peh (ed.), *Pitfalls in Diagnostic Radiology*,
DOI 10.1007/978-3-662-44169-5_17, © Springer-Verlag Berlin Heidelberg 2015

its strengths, weaknesses, and potential pitfalls. For example, ultrasound imaging has a central role in imaging the scrotum and is commonly used in assessing the kidneys and bladder; however, detecting air in the GU tract can be challenging with ultrasound imaging and is a source of pitfalls. CT is used for many indications related to the kidneys, ureters, and bladder, as well as the adrenal glands. However, there are many protocols to choose from which may affect diagnostic performance. MRI has a growing role in evaluation of the prostate, in addition to its established role in characterizing renal and adrenal lesions. MRI is not without limitations, including difficulty detecting parenchymal calcifications and calculi, as well as numerous imaging artifacts which can lead to diagnostic pitfalls.

A retrospective quality initiative project reviewing errors identified during follow-up imaging in the abdomen and pelvis over a 1-year period demonstrated that GU errors accounted for 14.7 % of all errors, second only to the liver (17 %). Within the GU tract, most (57 %) errors were as false-negative, 15 % were false-positive, and 14 % were cognitive errors (incorrect interpretation of a true finding) (Kielar et al. 2011). Several articles have described pitfalls in GU imaging (Israel and Bosniak 2008; Johnson et al. 2009; Sahdev et al. 2010). These include discussion of appropriate imaging techniques to highlight pathology, thereby reducing the number of false-negative errors. Others discuss potential similarities between abnormalities in the GU tract and ways of differentiating them: this could lead to a reduction in the number of false-positive errors and cognitive errors. In this chapter, each part of the GU system will be reviewed, focusing on pitfalls and strategies to deal with them.

17.2 Pitfalls in Imaging of the Adrenal Glands

The adrenal glands are small endocrine glands that are usually found just cranial to the kidneys, within the retroperitoneum. Given their unusual shapes, a common pitfall in cross-sectional imaging is volume averaging which can lead to the appearance of a focal lesion when none is present. Reviewing both axial and reformatted coronal images is helpful to prevent this pitfall.

17.2.1 Adrenal Pseudolesions

Pitfall: *Pseudolesions can be present in the vicinity of the adrenal glands*. These include splenic artery aneurysms, accessory spleens, renal masses, hepatic lesions, pancreatic lesions, and gastric diverticula (Gokan et al. 2005). Evaluation of the structures in two different planes (axial and coronal or sagittal) can help reduce false-positive errors associated with pseudolesions by determining their site of origin. In the case of gastric diverticula suspected on CT, administration of hyperdense oral contrast material to fill the diverticulum, or placing the patient prone to move air into the diverticulum, are easy problem-solving tools (Fig. 17.1a, b).

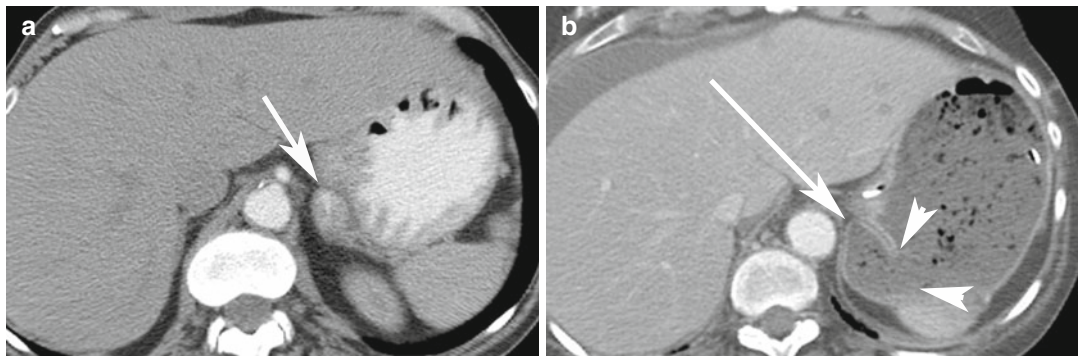

Fig. 17.1 Forty-five-year-old woman with incidental finding of a duodenal diverticulum next to the left adrenal gland. (**a**) Axial CECT image shows that the diverticulum is mostly decompressed, with only a trace of hyperdense oral contrast within it (*white arrow*). (**b**) Follow-up axial CECT image shows that the diverticulum is distended by food and fluid (*white arrow*). The neck of the diverticulum is clearly seen communicating with the stomach (*arrowheads*)

17.2.2 Adrenal Adenoma CT Pitfalls

Adrenal adenomas are common incidental findings, occurring in 5–7 % of elderly patients (Glazer et al. 1982; Song et al. 2008). On contrast-enhanced CT (CECT), there are overlapping imaging appearances between adrenal adenomas, metastases, and early primary adrenal malignancies; this is a frequent diagnostic dilemma when found incidentally (Boland et al. 1998; Johnson et al. 2009). Lee et al. (1991) were first to describe the finding of decreased density on non-enhanced CT (NECT) (densitometry) for the diagnosis of adenoma. Initial threshold levels of 0 Hounsfield Unit (HU) yielded specificity of 100 % but an unacceptably low sensitivity of only 47 % for the diagnosis of adenoma. Subsequently a higher threshold of 10 HU was identified through meta-analysis with sensitivity of 71 % while maintaining a high specificity of 98 % (Boland et al. 1998). *It is important to place the region-of-interest* (*ROI*) *measurement tools over one half to two thirds of the center of the lesion in order to reduce measurement error*. Placing a smaller ROI measurement can selectively underestimate the true density of a lesion. Placing the ROI measurement at the periphery of a lesion can result in decreased measurements due to averaging with retroperitoneal fat (Taffel et al. 2012) (Fig. 17.2a–e).

17.2.3 Adrenal Adenoma MRI Pitfalls

Mitchell et al. (1992) were the first to describe a loss of signal intensity with in- and opposed-phase or chemical shift gradient-echo imaging (CSI) for the diagnosis of adenoma. CSI is based on the principle that resonance frequencies of protons in water and lipid differ due to shielding effects from –CH2 groups within lipid molecules. The difference in precessional frequency can be exploited during gradient-echo imaging by selecting echo times (TE) where lipid and water protons will be in and out of phase with respect to each other. The chemical shift between water and lipid protons is 3.5 ppm (independent of field strength). This corresponds to a frequency shift of 220 Hz at 1.5 T and 440 Hz at 3 T. When lipid and water protons are in the same voxel but opposed (out of phase), there is signal cancellation in that voxel. The exact echo time for in- and opposed-phase CSI is dependent on field strength, with lipid and water protons becoming out of phase with each other once every 2.2 ms or 1.1 ms at 1.5 T and 3 T, respectively (Siegelman 2012).

Pitfall: *When assessing adrenal lesions for lipid content*, *the first out-of-phase echo should be sampled. If the second out-of-phase echo is sampled and compared to the shorter in-phase echo*, *then loss of signal on the out-of-phase images could be due to either lipid content or susceptibility* (*T2**) *effects from calcification or hemosiderin* (Siegelman 2012) (Fig. 17.3a, b). This is relatively straightforward at 1.5 T as current MRI systems are capable of performing dual-echo gradient-echo imaging during a single breath-hold with TE values of 2.2 and 4.4 ms. This requirement becomes more problematic at 3 T when sampling the first out-of-phase echo at 1.1 ms during the same breath-hold as the in-phase echo at 2.2 ms. Some vendors using older generation 3 T systems recommended sampling the first in-phase echo at 2.2 ms and the second out-of-phase echo at 3.3 ms. This strategy is suboptimal and can lead to the incorrect characterization of adrenal lesions, as described above.

The diagnosis of adrenal adenoma with CSI can be performed qualitatively by visually inspecting for a drop of single on opposed-phase images or by use of subtraction imaging (Siegelman 2012). Quantitative analysis can also be performed by calculating the chemical shift index ([signal intensity of lesion on in phase – signal intensity of lesion on opposed phase/signal intensity of lesion on in phase] × 100 %) or the adrenal-to-spleen chemical shift ratio ([signal intensity of lesion on opposed phase/signal intensity of spleen on opposed phase]/[signal intensity of lesion on in phase/signal intensity of spleen on in phase]), with respective values of >16.5 % and <0.71 being diagnostic of adenoma (Taffel et al. 2012). With CSI, the sensitivity and specificity for the diagnosis of adenoma range from 81–100 % to 94–100 %, respectively (Taffel et al. 2012).

Fig. 17.2 Seventy-eight-year-old woman with adrenal collision tumor; adrenal metastasis arising in a gland with a preexisting adenoma. (*Top row*) Baseline axial CECT images taken at time of diagnosis show a large right upper lobe non-small cell carcinoma (not shown) and a right adrenal nodule with homogeneous low density (*black arrow*) measuring −2 HU, diagnostic of adrenal adenoma. (*Middle row*) Follow-up axial NECT images performed 6 months later show a minute focus of increased density (*white arrow*) that has subsequently developed within the right adrenal gland (*black arrow*) which measures 20 HU in density. The remainder of the adrenal gland continues to show imaging characteristics and density values in keeping with adenoma. (*Bottom image*) Follow-up axial CECT image performed 5 months later shows bilateral enhancing adrenal masses in keeping with metastases. Heterogeneous low density with NECT or loss of signal intensity on CSI in a patient with underlying primary malignancy should alert the radiologist to the diagnosis of adrenal collision tumor

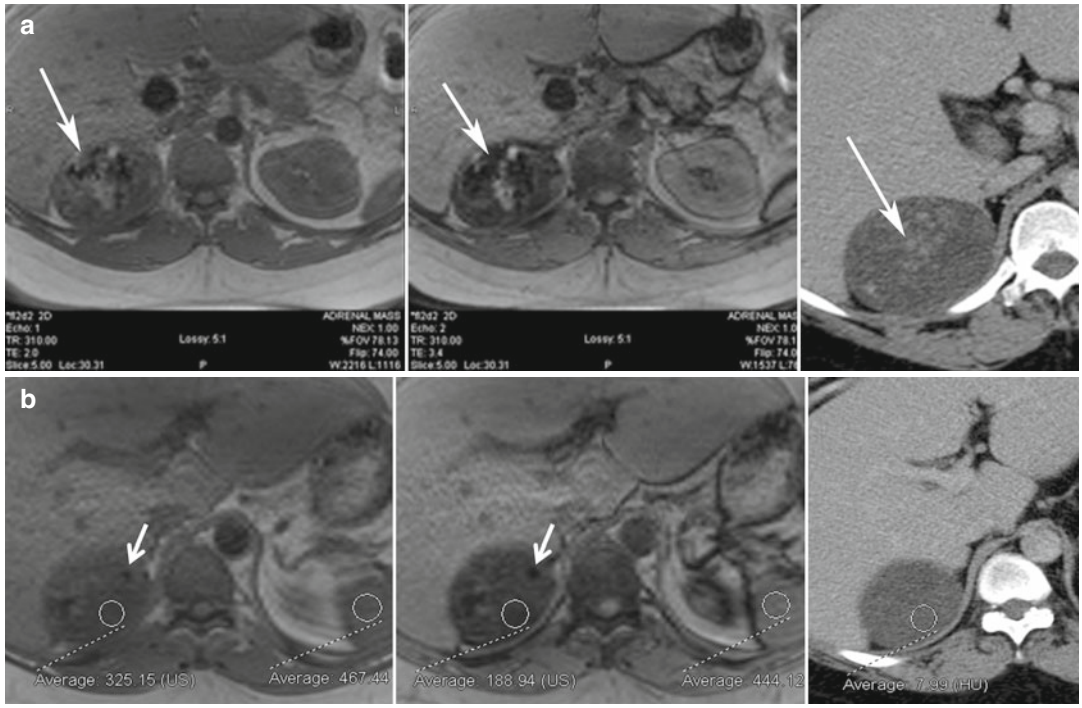

Fig. 17.3 Thirty-four-year-old man with proven adrenal cortical carcinoma following resection. (**a**) Axial in-phase (TE = 2.0 ms) and opposed-phase (TE = 3.4 ms) gradient-echo (GRE) MR images show the potential pitfall of chemical shift imaging at 3 T. When the opposed-phase image is compared to the in-phase image, there is a large area of decreased signal intensity (*white arrow*) related to calcifications within the tumor from T2* effects, which is confirmed in the axial CECT image. Another focus of calcification is noted in a separate portion of the mass (*white arrow*) with blooming artifact from T2* effects. When opposed-phase images are performed at a longer TE, drop in signal can be related to lipid or susceptibility artifact. (**b**) Other areas within the mass (ROI) show drop of signal intensity on the opposed-phase MR image and corresponding low density on CT (<10 HU) and represent areas of intracytoplasmic lipid. This can be diagnosed by visually assessing the signal intensity difference between the in- and opposed-phase MR images or by calculation of the adrenal index or adrenal-to-spleen signal intensity ratio. This illustrates an important imaging pitfall in adrenal imaging. Not all adrenal lesions that contain lipid are adenomas. Size, heterogeneity, and presence of calcification indicate that the adrenal mass in this patient is unlikely to represent adenoma, and diagnosis of adrenal cortical carcinoma was prospectively suggested at the time of diagnosis

Approximately 70 % of adrenal adenomas have sufficient intracytoplasmic fat content to be reliably diagnosed using either NECT or CSI. Conversely, 30 % of adrenal adenomas do not have high enough concentrations of lipid to be reliably diagnosed by either NECT or CSI and are referred to as "lipid-poor adenomas" (Boland et al. 1998). Both NECT and CSI exploit the same property of intracytoplasmic fat for diagnosis; therefore, CSI should offer no advantage in the diagnosis of adenomas that do not measure less than 10 HU in density on NECT (Boland et al. 1998). There is a slightly increased rate of diagnosis of adenoma with CSI compared to NECT (Haider et al. 2004), although for adrenal lesions that measure >25–30 HU on NECT, CSI is unlikely to be able to detect sufficient amounts of intracytoplasmic fat to diagnose an adenoma (Taffel et al. 2012). For adrenal lesions that are "lipid poor," adrenal washout CT can reliably differentiate adenomas from other lesions by enhancement patterns.

Pitfall: *Not all adenomas will not show signal drop on opposed-phase CSI*. In patients with

adrenal lesions that do not show signal loss on CSI, adrenal washout CT should be performed for further characterization (Boland et al. 1998). Studies have validated adrenal washout CT as an accurate imaging test for the diagnosis of both "lipid-rich" (those with sufficient lipid for diagnosis with NECT or CSI) and "lipid-poor" adenomas, with both types of adenoma having similar enhancement patterns (Taffel et al. 2012). Benign adenomas washout or de-enhance faster than malignant adrenal lesions, presumably related to the disorganized angiogenesis in malignancy which leads to prolonged contrast accumulation (Taffel et al. 2012). Adrenal washout CT should be performed after a standard contrast-enhanced 60 s portal venous phase (PVP) delay and 15 min post-contrast delay, with or without NECT. Calculation of HU ratios can be *relative* (enhanced – delayed/enhanced × 100 %) or *absolute* (enhanced – delayed/enhanced – unenhanced × 100 %) with values >60 % or >40 % diagnostic of adenoma, respectively (Boland et al. 1997; Korobkin et al. 1998; Caoili et al. 2000). Ten-minute delays have also been studied to decrease imaging time but have decreased diagnostic accuracy when compared to 15 min delays (Blake et al. 2006; Taffel et al. 2012).

17.2.4 Pheochromocytoma CT Pitfalls

Pitfall: *Pheochromocytomas may demonstrate washout on adrenal CT washout studies*. Pheochromocytoma is a rare primary adrenal neoplasm, found in 0.1–0.2 % of patients with hypertension. These vascular neoplasms may demonstrate similar CT washout kinetics as benign adenomas but in contradistinction to adenomas, pheochromocytomas have marked absolute enhancement on the 60 s PVP scan. If the absolute ROI attenuation on PVP exceeds 100 HU, one should strongly suspect a diagnosis of pheochromocytoma, regardless of the % washout at 15 min (Boland et al. 1997) and clinical workup should be initiated.

17.2.5 India Ink Artifact

Pitfall: *India ink artifact can mimic signal drop on CSI in very small lesions*. Opposed-phase gradient recalled echo images demonstrate chemical shift artifact of the second kind, also called "India ink" artifact at fat-water boundaries. This artifact is due to the presence of an admixture of fat and water protons (from two different tissues) within the same imaging voxel, resulting in a drop of signal when protons are out of phase (Delfaut et al. 1999). It is important not to confuse India ink artifact at the boundary of an adrenal lesion and retroperitoneal fat as signal drop within the adrenal lesion. This can result in the erroneous diagnosis of adenoma and can be particularly problematic for very small adrenal lesions.

17.2.6 Lipid-Containing Adrenal Tumors

Pitfall: *Not all adrenal lesions that lose signal on CSI are benign adenoma*s. Lipid-containing primary tumors such as clear cell renal cell carcinoma (ccRCC) and hepatocellular carcinoma (HCC) can metastasize to the adrenal glands, though usually these are advanced cases. These metastases may demonstrate a loss of signal with CSI and can mimic adenomas (Shinozaki et al. 2001; Sydbow et al. 2006). Typically, this is not an imaging quandary as patients are known to have an underlying primary malignancy, and adrenal lesions will either develop de novo or demonstrate rapid growth on follow-up imaging. Choi et al. (2013) recently demonstrated that adrenal washout CT is not a reliable means to differentiate metastases from HCC or ccRCC from adenoma, advising follow-up if this diagnosis is being considered. Rarely, primary adrenal neoplasms, such as adrenal cortical carcinoma and pheochromocytoma, can also contain intracytoplasmic lipid and demonstrate low density on NECT and loss of signal on CSI, mimicking adenoma. Differentiation from adenoma is based on clinical symptoms, laboratory investigations and additional imaging features such as size, heterogeneity, and calcification (Blake et al. 2003; Elsayes et al. 2004).

17.2.7 Adrenal Collision Tumor

Pitfall: *Heterogeneous low density on NECT or loss of signal intensity on CSI in a patient with known malignancy can rarely be due to an adrenal collision tumor*. Case reports exist of adrenal metastases arising within an adrenal gland that contains a preexisting benign adrenal adenoma. In a study of 104 patients with known primary malignant tumor and an adrenal mass, 2 % of cases had a collision tumor (Schwartz et al. 1996). These tumors are important to recognize, particularly if biopsy is being planned, since the potentially malignant portion of the mass should be selectively sampled for adequate diagnosis (Fig. 17.2a–e).

17.3 Pitfalls in Imaging the Kidneys

All imaging modalities have a role in renal imaging, depending on the clinical indication. It is estimated that there are more than 1.2 million visits to the emergency department (ED) yearly in USA for acute flank pain (Pitts et al. 2008). This can be due to renal calculi, trauma, infections, neoplasms, as well as nonrenal causes. Evaluation can be done with ultrasound imaging or CT, depending on patient's age, body habitus, and institutional availability of imaging modalities. For ultrasonographic evaluation, optimal operator technique is required, including adjusting the depth of imaging and the location of the focal spot to be at or just behind the area of interest, as well as patient factors including the ability to hold their breath. Calculi can be identified on ultrasound imaging as echogenic foci which demonstrate shadowing behind them, though calculi can be missed due to small size, surrounding echogenic renal sinus fat and patient factors such as large body habitus.

17.3.1 Twinkling Artifact

An aid to identifying renal calculi is the "twinkling artifact." The "twinkling artifact" appears as a rapidly alternating color Doppler signal that imitates turbulent flow, often identified behind a strongly reflecting, irregular interface, such as a renal calculus (Rahmouni et al. 1996) (Fig. 17.4a, b). In order to evaluate confirm a twinkling artifact, a high pulse repetition frequency should be chosen to eliminate Doppler signal from vascular structures. A Doppler spectrum of the area of twinkling demonstrates a broadband aliasing signal consistent with noise produced by the reflected signal. In a prospective study in patients with flank pain, the positive predictive value (PPV) of twinkling artifact for identifying calculi was 94 %. In comparison, PPV of grayscale US for detecting urinary tract calculi was only 65 % (Kielar et al. 2012).

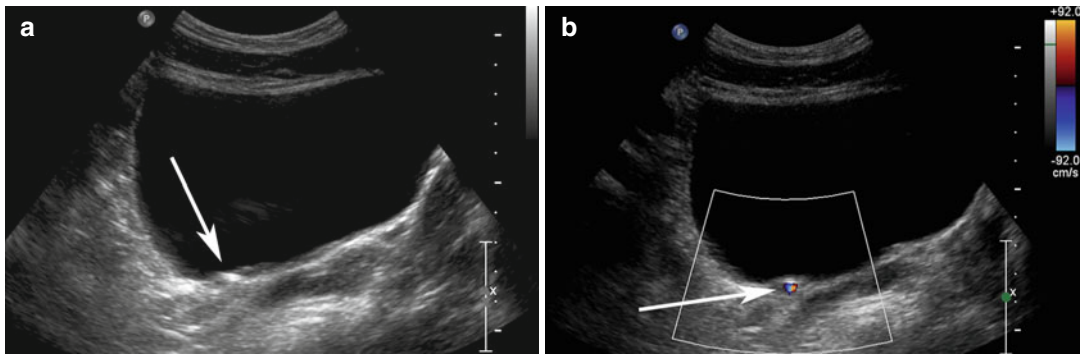

Fig. 17.4 (**a**) Transverse ultrasound image of the bladder shows an echogenic structure at the right UVJ (*arrow*) which could represent a calculus, but there is no definite shadowing behind it. (**b**) When color Doppler is turned on with high pulse repetition frequency (92 cm/s at *top right* of image), the twinkling artifact is readily identified behind the calculus (*arrow*)

17.3.2 Renal Pseudotumors

Pitfall: *On ultrasound imaging*, *pseudotumors such as columns of Bertin and dromedary humps*, *as well as focal infarcts and focal bacterial pyelonephritis*, *can present as mass-like abnormalities in the kidney* (Tsuji et al. 2007). A column of Bertin is a normal variant of unresorbed parenchyma of one or both of the two sub-kidneys that fuse in fetal development to form a normal kidney (Bhatt et al. 2007). It projects into the renal sinus, splaying the sinus. A dromedary hump is a focal bulge of the lateral border of the left kidney as the kidney adapts to the shape of the adjacent spleen (Bhatt et al. 2007). These variants can usually be diagnosed on ultrasound imaging as being normal, since there is no loss of expected differentiation between the cortex and medulla, despite their unusual location or shape. For diagnosis of infarcts, focal pyelonephritis and other nonspecific mass-like areas, CECT is frequently used for characterization. Both focal pyelonephritis and infarcts can demonstrate areas of reduced enhancement on CECT (Tsuji et al. 2007) (Figs. 17.5a, b and 17.6a, b).

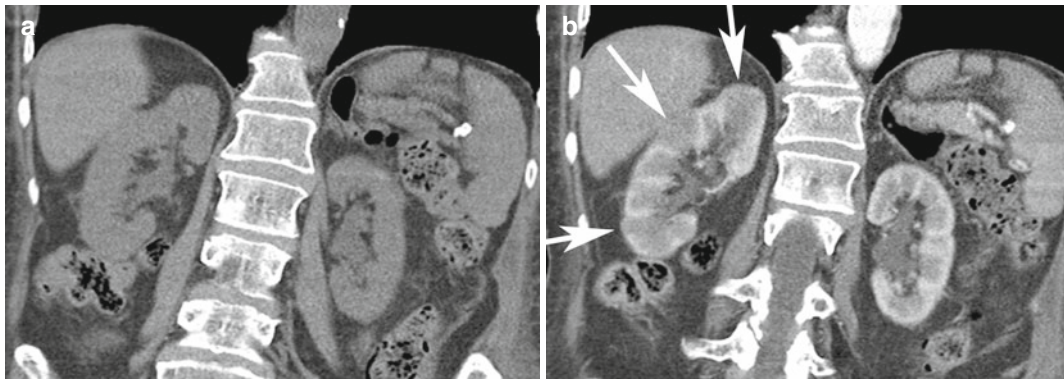

Fig. 17.5 Forty-four-year-old patient with right flank pain. (**a**) Coronal NECT image does not show any hydronephrosis or calculus on the right. Due to severity of symptoms, a CECT was performed. (**b**) Coronal CECT image shows focal areas of reduced cortical enhancement (*white arrows*) in keeping with acute pyelonephritis. The patient had positive urine cultures and recovered after antibiotic therapy

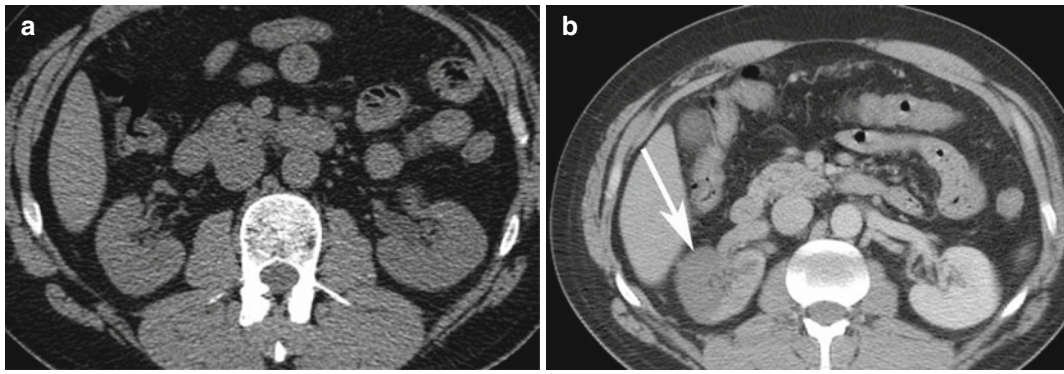

Fig. 17.6 Thirty-seven-year-old IV drug user with sudden onset of severe right flank pain. (**a**) Axial NECT image does not show any hydronephrosis on the right side or other causes of pain. Due to a new cardiac murmur and concern for endocarditis, a CECT was performed on the same day. (**b**) Axial CECT image shows a geographic area of non-enhancement in the right kidney consistent with an infarct (*arrow*). A subsequent echocardiogram revealed vegetation in the left ventricle, consistent with endocarditis. This was the source of emboli to the kidney

17.3.3 CT of Flank Pain

When choosing CT to investigate flank pain, patient radiation exposure, slice thickness, and image noise can affect detection of small calculi. Though NECT is the gold standard in urolithiasis imaging, with a reported sensitivity greater than 93 % and specificity of 100 %, attention to technical parameters is advised (Kim et al. 2005). Jin et al. (2009) reported a low sensitivity (80 %) for small stones (2–4 mm) when using 5 mm slices; thinner sections are therefore necessary for the best diagnostic accuracy.

Pitfall: *In patients with flank pain but no renal calculus identified*, *false-negative or satisfaction-of-search errors can occur unless alternative diagnoses are actively sought*. Ahmad et al. demonstrated that 68 % of patients presenting to the ED with flank pain were found to have calculi or recently passed calculi on NECT (Ahmad et al. 2003). In their population, 12 % had other diagnoses identified on NECT, including appendicitis, diverticulitis, pancreatitis, and ovarian pathology (Ahmad et al. 2003). Other studies have shown that up to a third of patients will have other diagnoses detected on NECT (Colistro et al. 2002).

Pitfall: *In patients with flank pain but no renal calculus on NECT*, *renal parenchymal abnormalities can be missed*. Clinically overlapping etiologies affecting the kidney can be missed if intravenous contrast agent is not administered. If no diagnosis is identified in the kidney or elsewhere in the abdomen on NECT and symptoms are concerning (e.g., fever, pain out of proportion to findings, underlying risk factors for a hypercoagulable state), CECT should be considered to exclude renal infarcts and infiltrating renal masses such as lymphoma and leukemia. Pyelonephritis is usually diagnosed clinically; however, within the imaging spectrum of patients with possible pyelonephritis (Fig. 17.5a, b), lymphoma can have overlapping CT appearances. Both pathologies can present with fever and leukocytosis, and in immunocompromised patients, typical symptoms of pyelonephritis, including flank pain, can be diminished or absent. Patients with renal infarction can have a high white cell count, high creatinine, and gross or microscopic hematuria which overlaps clinically with renal calculi (Chu et al. 2006) (Fig. 17.6a, b).

17.3.4 Hydronephrosis Mimics

Pitfall: *Parapelvic cysts and peripelvic cysts can mimic the appearance of hydronephrosis*. There are imaging tips which can help differentiate these etiologies. Parapelvic cysts, which arise from the renal parenchyma and protrude into the collecting system, are often round or oval and do not communicate with one another (Zinn and Becker 1997). Peripelvic cysts can arise from ectasia of renal sinus lymphatics and can also simulate hydronephrosis, but these often also have convex walls and oval shapes. Peripelvic cysts are often bilateral and patients do not have symptoms of obstruction. In hydronephrosis, there is communication of the renal pelvis with the dilated collecting system. The dilated calyces follow their expected shape, except that they have a more blunted appearance (Zinn and Becker 1997). CT urography can reliably differentiate hydronephrosis from parapelvic and peripelvic cysts by demonstrating the presence of excreted contrast material passing between cystic spaces into a non-dilated renal pelvis in the case of parapelvic and peripelvic cysts; however, CT urography is seldom required for this purpose.

A rare consideration in the differential diagnosis of hydronephrosis includes renal arteriovenous malformation (AVM). Doppler interrogation is key, as it demonstrates vascular, arterial, and mosaic vascular flow within the anechoic areas (Muraoka et al. 2008). On CECT, arterial imaging demonstrates brisk enhancement, but if only delayed imaging is obtained. This diagnosis could be misinterpreted as slow excretion of contrast material in moderate hydronephrosis, since the AVM would have the same density as the inferior vena cava (IVC). Finally, if a patient presents with new hydronephrosis, the cause should be identified. Particularly in older patients with new "ureteropelvic junction (UPJ) obstruction," images should be carefully scrutinized

since malignant causes such as transitional cell carcinoma (TCC) or metastases from other primaries need to be excluded (Kane et al. 2012).

17.3.5 Angiomyolipoma and Mimics

Angiomyolipoma (AML) is a benign renal neoplasm which is composed of variable amounts of fat, smooth muscle, and blood vessels. Differentiation of AML from other solid renal masses is important because unnecessary surgery can be prevented. The imaging diagnosis of AML hinges on the detection of gross fat (often referred to as "macroscopic fat") within the lesion. This can be readily diagnosed with CT by detection of areas within the lesion that measure less than −20 HU which is diagnostic of gross or "macroscopic" fat content (Sasiwimonphan et al. 2012). On MRI, gross fat can be detected as a loss of signal intensity on gradient-echo or spin-echo pulse sequences performed with chemically selective or spectral fat suppression. As opposed to the intracytoplasmic fat within adrenal adenomas (discussed earlier), gross or "macroscopic" fat does not lose signal intensity with CSI because imaging voxels contain only fat protons and there is no phase cancellation. A renal AML can however be diagnosed on opposed-phase gradient-echo MRI by observing the India ink artifact at the fat-water interfaces between the lesion and adjacent kidney parenchyma, or lack of such an artifact at interfaces between the lesion and retroperitoneal fat. AML is often incidentally identified on ultrasound imaging, appearing echogenic due to their fat content, although the ultrasonographic appearance is not pathognomonic.

Pitfall: *Not all echogenic renal nodules on ultrasound imaging are AMLs*. Occasionally, renal cell carcinoma can present as an echogenic nodule. Therefore, echogenic renal nodules often require further evaluation with CT or MRI to evaluate for the presence of gross fat (Farrelly et al. 2008; Marhuenda et al. 2008). In younger patients with a low risk of malignancy, follow-up ultrasound imaging to confirm stability may also be considered (Fig. 17.7a–d).

Pitfall: *Malignant renal neoplasms*, *including clear cell and papillary carcinoma*, *have been noted to rarely contain gross or "macroscopic" fat* (D'Angelo et al. 2002; Garin et al. 2007). In these instances, although exceedingly rare, imaging differentiation from AML is very challenging. The presence of intralesional calcification favors renal cell carcinoma since calcification is exceedingly rare in AML (but has also been reported) (Merran et al. 2004). Thus, in an unusual or aggressive-appearing renal mass which contains macroscopic fat, consider the rare possibility of fat within a malignant renal neoplasm (Fig. 17.8).

Pitfall: *In approximately 5 % of AMLs*, *there is insufficient fat to be detected by the CT and MRI methods described above* (Sasiwimonphan et al. 2012). These lesions are often referred to as "minimal fat" AML. Various imaging findings have been studied for the preoperative diagnosis of these lesions, such as a loss of signal intensity with CSI, homogeneously low T2 signal intensity, and enhancement characteristics with mixed results (Hindman et al. 2012). In one study, use of CSI was able to reliably diagnose "minimal fat" AML from other lesions by detecting a larger drop of signal intensity on opposed-phase gradient-echo MRI when compared to other renal masses (Kim et al. 2006). Subsequent studies have been unable to reproduce these findings due to overlap with some clear cell renal cell carcinomas (Hindman et al. 2012).

Pitfall: *Some clear cell renal cell carcinomas will demonstrate loss of signal intensity with CSI due to intracytoplasmic fat*. Potential overlap between ccRCC with intracytoplasmic fat and minimal fat AML can result in the erroneous diagnosis of a benign entity in the setting of primary renal malignancy (Yoshimitsu et al. 1999). Homogeneously low intensity on T2-weighted MR images in the setting of a renal lesion with loss of signal on CSI would favor "minimal fat" AML, although this finding has yet to be validated on a large scale (Hindman et al. 2012). A renal neoplasm without gross or "macroscopic" fat and with loss of signal intensity on CSI can be either a "minimal fat" AML or ccRCC and should be considered potentially malignant until proven otherwise (Fig. 17.9).

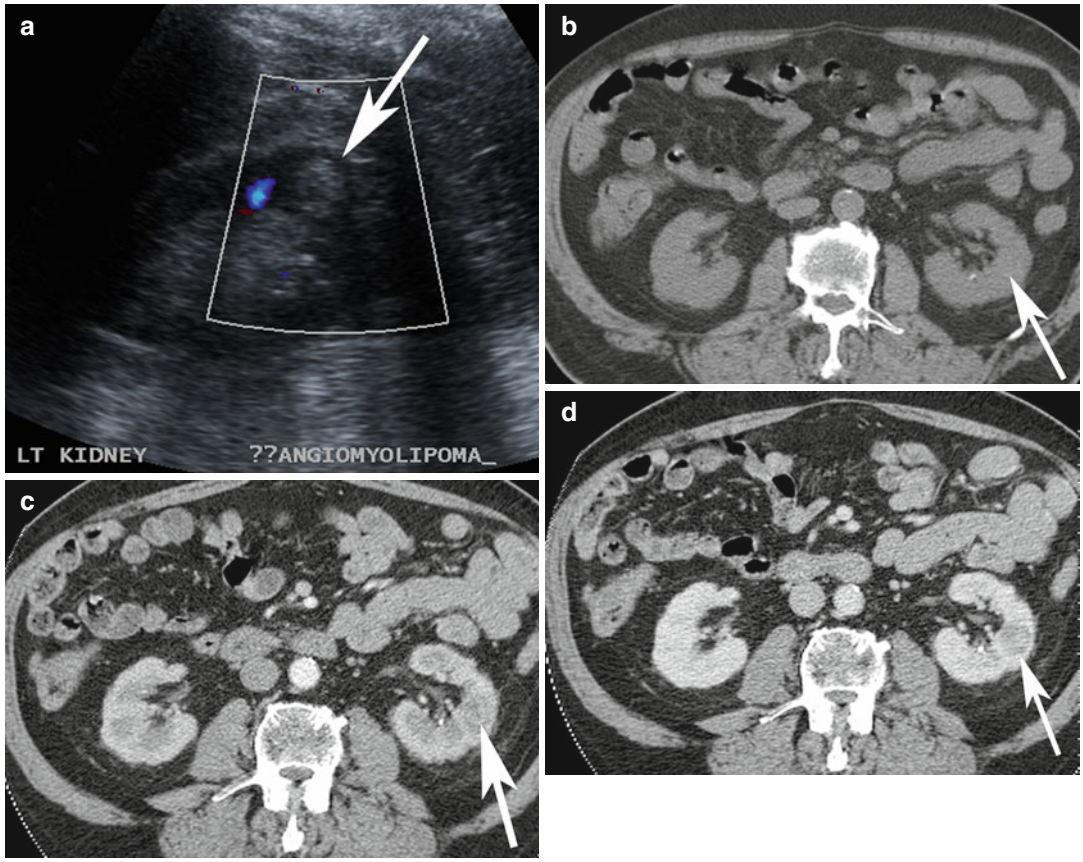

Fig. 17.7 (**a**) Ultrasound image of a 65-year-old patient shows incidental finding of an echogenic lesion in the cortex of the left kidney which was originally considered to represent an AML (*arrow*). (**b**–**d**) Axial multiphase (**b**) non-enhanced, and contrast-enhanced (**c**) arterial and (**d**) nephrographic phase CT images show that there is no macroscopic fat in the lesion and there is washout in the nephrographic phase. This lesion was resected and confirmed to be a renal cell carcinoma

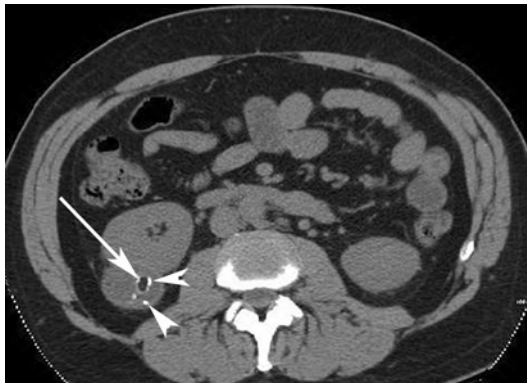

Fig. 17.8 Axial NECT image of a patient with an exophytic lesion in the right kidney (*arrow*) which has macroscopic fat but also contains calcifications (*arrowheads*). CECT (not shown) showed significant enhancement and washout. Surgical resection revealed a renal cell carcinoma with macroscopic fat and calcifications, which is a rare finding

17.4 Pitfalls in Imaging of the Ureters

Ureters are conduits for urine between the kidneys and the bladder. They travel in the retroperitoneum next to arteries, veins, muscles, and lymph nodes. They are long and of small caliber, making assessment challenging.

17.4.1 Ureteric Calculus Mimics

Pitfall: *Particularly in thin patients with minimal retroperitoneal fat*, *differentiation between a ureteric calculus and an atherosclerotic plaque or pelvic phlebolith on CT can be challenging*. Helpful findings favoring a ureteric calculus

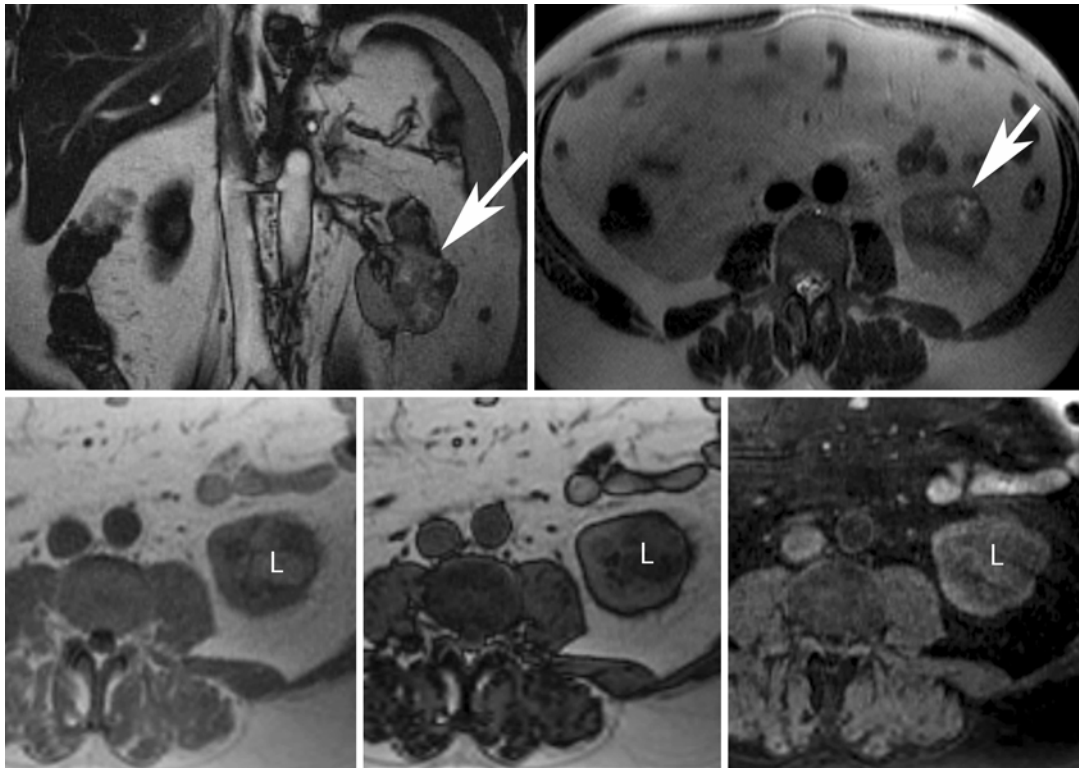

Fig. 17.9 Fifty-four-year-old man with proven clear cell renal cell carcinoma following resection. (*Top row*) Coronal balanced steady-state free precession (bSSFP) (*left*) and axial T2-W single-shot fast spin-echo (ssFSE) (*right*) MR images show an exophytic left renal mass with heterogeneously increased T2 signal intensity (*white arrows*). (*Bottom row*) Axial in- and opposed-phase GRE and T1-W spectral fat-saturated 3-D GRE MR images show the presence of intracytoplasmic lipid (*L*) within the mass revealed by signal loss on the opposed-phase image (*middle*) but not on the spectral fat-saturated sequence (*right*). Note that macroscopic or gross fat demonstrates loss of signal with spectral fat suppression but remains bright on opposed-phase images. Some clear cell renal cell carcinomas may contain intracytoplasmic lipid and cannot be reliably differentiated from "minimal fat" AML. The heterogeneous loss of signal intensity on opposed-phase GRE and areas of T2 hyperintensity within the mass favors a diagnosis of carcinoma

include perinephric and periureteric stranding as well as the "rim sign" around the calculus (Heneghan et al. 1997; Arac et al. 2005). The "rim sign" represents the muscular ureteric wall which surrounds a calculus. Phleboliths are calcified concretions within a vein wall as a result of thrombosis. The wall of the vein is thinner than the wall of the ureter and thus a rim is not visible around a phlebolith. A central lucency has been a described in vascular phleboliths on radiographs; however, this appearance is uncommonly seen on CT and cannot be reliably used to differentiate the two (Kim 2001). In cases where the ureter is in close contact with an atherosclerotic vessel, evaluation on coronal images often demonstrates the length of the atherosclerotic plaque along the artery. However, in instances where the plaque is focal, the diagnostic dilemma of a non-obstructive ureteric calculus can persist. In these rare cases, an excretory phase of a CECT can be used to demonstrate flow of urine through the decompressed ureter, next to the atherosclerotic plaque (Fig. 17.10a, b). In the unlikely case of a non-obstructive calculus, the hyperdense urine would flow around the calculus, surrounding it.

Pitfall: *In patients with hydroureter and soft tissue density material in the ureter at the site of obstruction*, *blood clots from recently passed calculi and transitional cell carcinoma* (*TCC*) *can have overlapping appearances on NECT*.

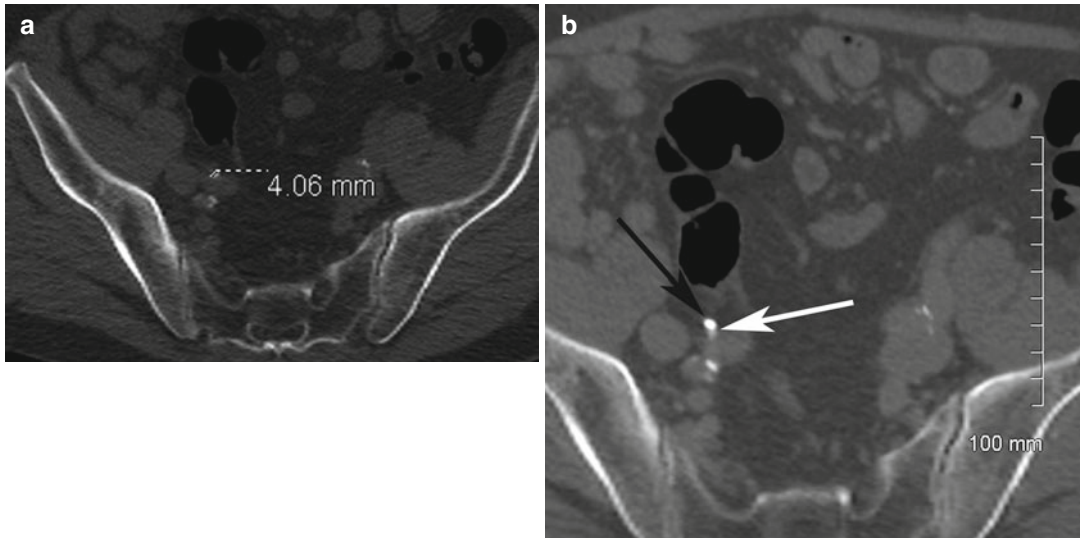

Fig. 17.10 (**a**) Axial NECT performed for right flank pain. The calcified structure was initially misinterpreted as a calculus in this thin patient with mild atherosclerotic changes. There was no proximal hydronephrosis. (**b**) The patient underwent CT urography a few weeks later for other reasons. Excreted contrast material within the ureter is located posterior (*white arrow*) to the calcification (*black arrow*), confirming that this structure represents an atherosclerotic plaque rather than a calculus

Identification of the area of transition is important; however, differentiation between these entities may not be possible, even with adequate clinical history and symptoms since both of these conditions can present with hematuria and clots (Khan and Lin 2013). In these cases, ureteroscopy may be required for direct visualization and sampling.

17.4.2 CT Urography Pitfalls

CT urography is a technique for evaluating the urinary tract with positive contrast opacification. It is commonly used to investigate hematuria in patients at risk for TCC but can be used in surveillance of patients his prior history of urothelial cancer, those with hydronephrosis of unknown cause and for evaluation of anatomic ureteric variants (Silverman et al. 2009). Though techniques vary, many institutions perform a double injection – the "split-bolus" technique. This allows a single scanning phase in order to evaluate the renal parenchyma during the nephrographic phase (100 s after intravenous administration of intravenous contrast material) while at the same time viewing the already opacified renal collecting system and ureters (Silverman et al. 2009).

Pitfall: *A common imaging pitfall in CT urography includes incomplete filing of the ureters with the excreted contrast material*. Encouraging patient hydration, intravenous hydration, and use of furosemide has been described in the literature, but none of these techniques guarantee complete opacification of the entire course of the ureters. Repeat imaging (occasionally in prone position) to visualize unopacified segments in patients at risk for TCC must be weighed against the risk of radiation exposure. Careful scrutiny of each renal calyx on axial and coronal reconstructed images is mandatory since small lesions can be subtle, leading to false-negative errors. Using window levels similar to bone windows helps to show filling defects in the dense excreted contrast material, which may otherwise be obscured if "abdominal window" settings are used. TCC can present as focal filling defects, areas of circumferential urothelial thickening or in more advanced cases, as masses. In a study by Caoili et al. (2005), 24/27 (88 %) of urothelial tumors were retrospectively identified using the CT urography technique (Fig. 17.11a, b).

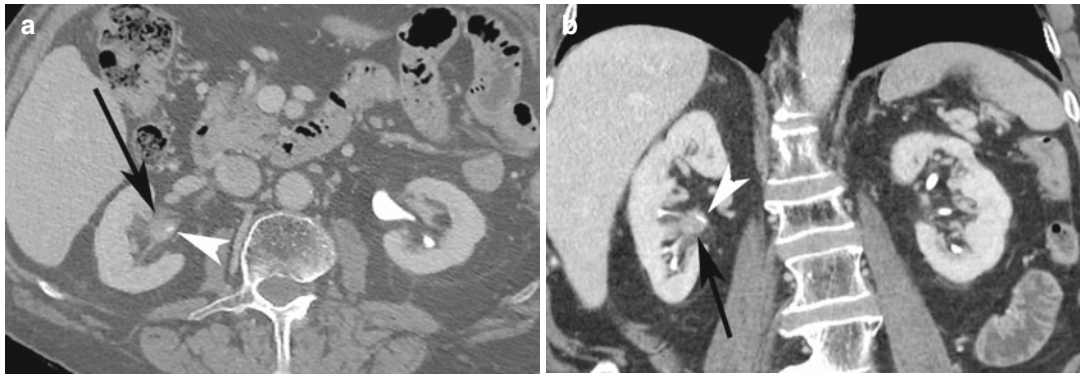

Fig. 17.11 (**a**) Axial and (**b**) coronal CECT images in a patient with right-sided transitional cell carcinoma. The *black arrow* indicates focal thickening of the urothelium due to tumor. The *white arrowhead* outlines the excreted contrast material

17.4.3 MR Urography Pitfalls

MR urography can also be used for diagnosis of TCC and anatomic abnormalities, though it has more technical challenges to produce high-quality images, and MRI is not as accessible as CT in many centers. MRI has higher contrast resolution in soft tissues compared to CT and since it does not use ionizing radiation, MR urography has been successfully investigated in pediatric populations to depict a wide range of congenital abnormalities of the kidneys, ureters, and bladder (Avni et al. 2002; Grattan-Smith and Jones 2006). However, the continuing challenge of MR urography is to obtain diagnostic quality images in a reasonable amount of time within the limits of respiration, peristalsis of ureters, flow artifacts of moving urine, and artifacts from bowel peristalsis nearby. These impediments are being overcome with faster and more robust imaging techniques; thus, this imaging modality may become more mainstream in the near future.

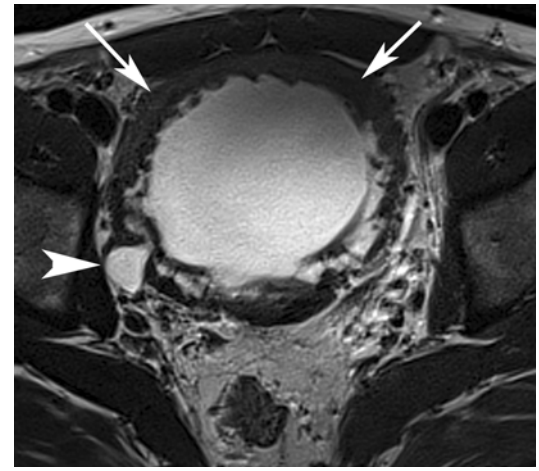

Fig. 17.12 Axial T2-W MR image of a 29-year-old man with neurogenic bladder and resultant bladder wall thickening (*white arrows*) and diverticulum (*white arrowhead*). This patient had chronic prostatitis (see Fig. 17.19a, b)

17.5 Pitfalls in Bladder Imaging

This reservoir for urine can be completely decompressed or fully distended during imaging; in some patients with chronic outlet obstruction, the bladder can have measured volumes of greater than 1 L (Fig. 17.12). In a mostly decompressed state, the bladder can have only a few dependent areas filled with urine; these can be misinterpreted as an abscess or pseudolesions due to volume averaging.

17.5.1 Bladder Diverticula Mimics

Pitfall: *Bladder diverticula can be misinterpreted as cystic or necrotic structures in the pelvis*, *particularly in patients being investigated for recurrence of pelvic malignancies* (Fig. 17.13a, b).

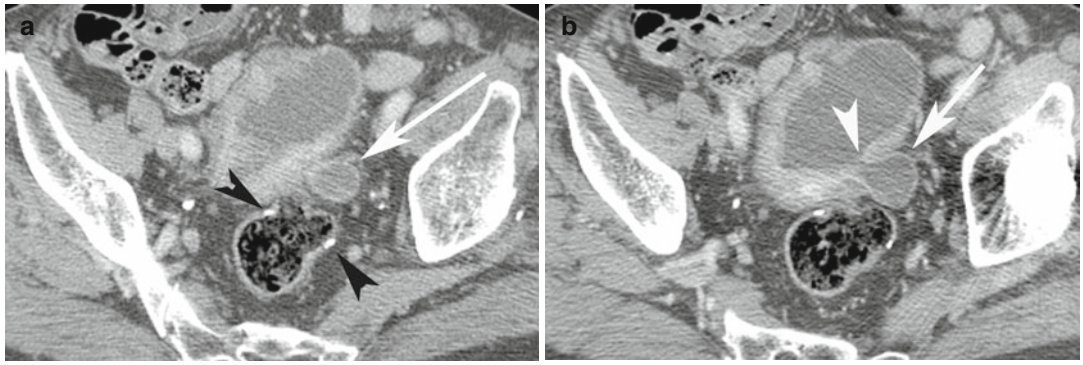

Fig. 17.13 Sixty-seven-year-old man with history of CRC and previous rectal resection (*black arrowheads*). (**a**) Axial CECT image shows a central low-density structure (*white arrow*) near the anastomotic line which could be misinterpreted as a necrotic lymph node. (**b**) Careful inspection of the axial CT image taken at another level shows the communication between the bladder (*white arrowhead*) and this diverticulum (*white arrow*)

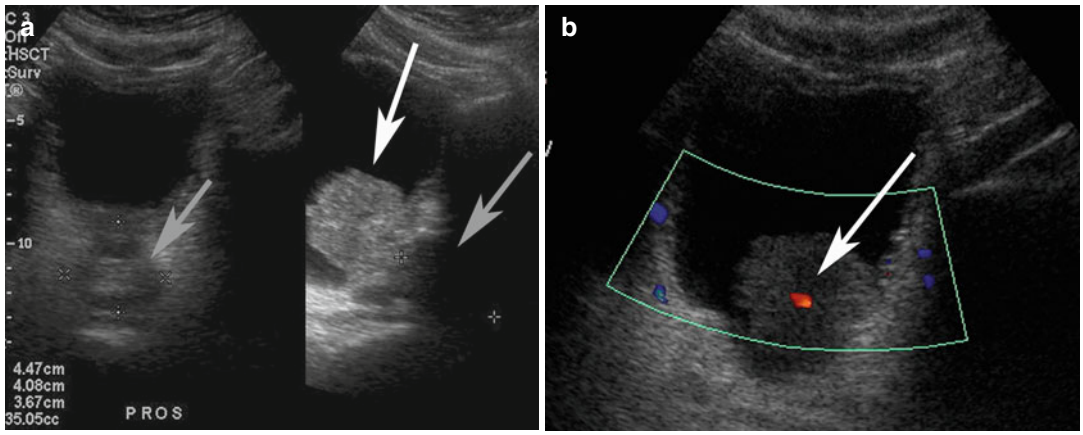

Fig. 17.14 (**a**) Transverse (*left*) and sagittal (*right*) ultrasound images of the bladder in a patient with a midline soft tissue mass. The prostate is depicted in the left image and the mass appears to be of different echogenicity than the bladder and slightly off midline. (**b**) Doppler ultrasound image of the bladder mass shows flow within it. This was biopsy-proven to be a transitional cell carcinoma

Careful evaluation for a communication between the diverticula and the bladder both on axial and coronal images, comparison with previous imaging, and assessing the bladder for bladder trabeculations or other diverticula can help prevent a false-positive diagnosis. Ultrasound imaging can also be used for problem solving in such cases. The bladder can be imaged full and after voiding to see if the structure persists. In addition, real-time imaging can identify urine jets into the diverticulum using color Doppler (Levine and Filly 1994; Maynor et al. 1996).

17.5.2 Transitional Cell Carcinoma Mimics

Pitfall: *Differentiating TCC from blood clot or from mass effect of the central lobe of the prostate at the base of the bladder can be challenging both on ultrasound imaging and CT*. Endophytic TCC can often be differentiated from adherent clot on ultrasound imaging due to the presence of vascular flow in the neoplasm, which is not present in clots or debris (Fig. 17.14a, b). Presence of a TCC at the base of the bladder can

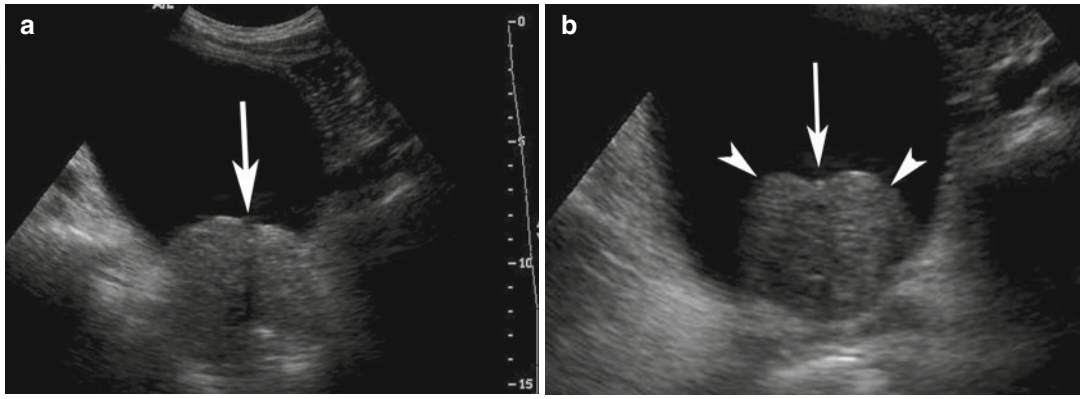

Fig. 17.15 (**a**, **b**) Two ultrasound images of the bladder in a patient with suspected bladder mass. The mass is contiguous with the prostate and of same echogenicity (*arrowheads*). Centrally, the urethra is identified (*arrow*) indicating that this is simply a mass effect of the enlarged central gland of the prostate in a patient with benign prostatic hypertrophy

be more challenging to differentiate from the prostate gland, based solely on vascularity, since both structures will have a blood supply. However, identification of the urethra in the center of the protruding prostate, particularly in patients who have undergone transurethral prostate resection (TURP) as a treatment for bladder outlet obstruction, increases confidence that the structure represents prostatic tissue rather than TCC (Fig. 17.15a, b).

17.5.3 Bladder Rupture Pitfalls

Pitfall: *In a trauma patient with pelvic injuries*, *a bladder rupture can be missed on standard CECT*. Bladder ruptures can be intraperitoneal or extraperitoneal and are often associated with adjacent hematoma or free fluid (urine). When extraperitoneal, the fluid often accumulates in the space of Retzius, anterior to the bladder. Extraperitoneal bladder rupture is often managed with simple catheterization and healing rarely requires additional intervention. Treatment of intraperitoneal bladder rupture often requires surgical exploration and repair, since the urine takes the path of least resistance and continues to leak into the peritoneal cavity (Corriere and Sandler 1986). The risk of bladder injury is related to the degree of bladder distention at the time of the trauma, and it is often associated with pelvic bone fractures. To prevent missing a focal bladder disruption and to correctly diagnose the type of rupture, a CT cystogram should be performed after instilling of a minimum of 300 ml of diluted contrast material (e.g., 50 ml of Hypaque 60 [Nycomed, Princeton NJ] and 450 ml of normal saline solution) through a Foley catheter using gravity (Vaccaro and Brody 2000) (Fig. 17.16a, b). Delayed imaging of excreted contrast material into the bladder after a standard contrast-enhanced CT scan is not sufficient to exclude a bladder rupture; this is comparable to looking at a bicycle inner tube for a puncture without first filling the tube with air.

17.5.4 Bladder Air Pitfalls

Pitfall: *Air in the lumen of the bladder can be introduced during catheterization*, *though history of intermittent catheterization is not always provided*. This can lead to a false-positive pitfall of diagnosing either emphysematous cystitis or a fistulous connection with a bowel loop. Lack of bladder wall thickening, perivesical fat stranding, air within the bladder wall, and clinical symptoms of sepsis should allow for differentiation of infection from simple air introduced during catheterization (Tsai et al. 2012). Careful scrutiny of nearby small bowel loops and colon is important to exclude a fistula, though this is rarely an incidental finding, since patients often present with pneumaturia.

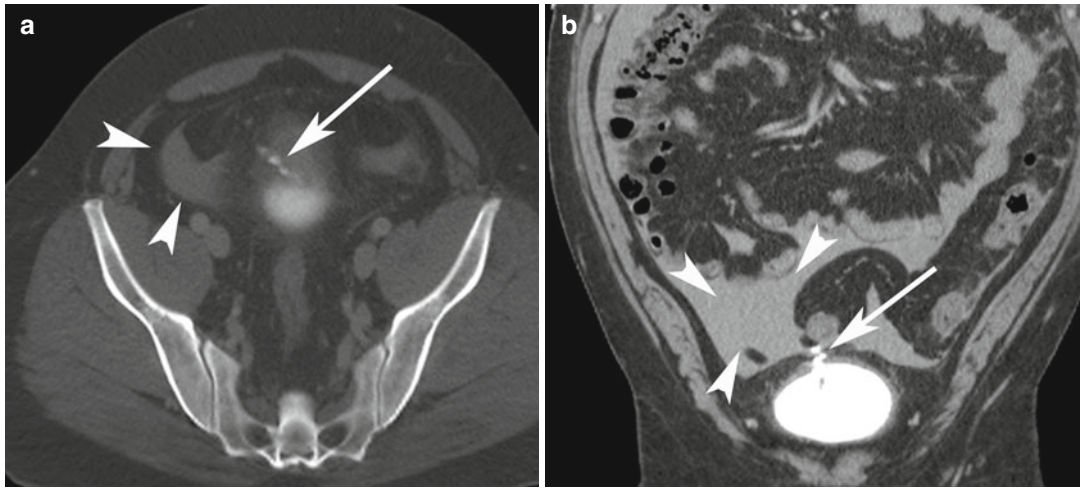

Fig. 17.16 Twenty-two-year-old patient who was hit by a car. Three hundred milliliters of water-soluble contrast agent was instilled into the bladder through a Foley catheter as part of a CT cystogram. (**a**) Axial CT image shows a tiny leak of fluid from the dome of the bladder (*arrow*). There is free fluid in the peritoneum (*arrowheads*). (**b**) Coronal CT image in the same patient shows the small defect in the bladder (*arrow*) which could be missed if a formal CT cystogram was not attempted. Free peritoneal fluid (*arrowheads*) is present

17.6 Pitfalls in Prostate Imaging

Ultrasound imaging is used for measuring prostate volumes and for guiding prostate biopsies. However, sensitivity and specificity of ultrasound imaging for detecting prostate cancer is low (Catalona et al. 1994). MRI is widely accepted as the best imaging modality for local staging of disease in patients with biopsy-proven prostate cancer, for detecting local recurrence after prostate cancer therapy, and is increasingly being used for localizing and grading tumors in patients with negative prostate biopsies but with rising prostate-specific antigen (PSA) and those on active surveillance (Lawrentschuk and Fleshner 2009). High spatial resolution turbo spin-echo (TSE) T2-weighted MR imaging with a pelvic or endorectal coil has been previously validated for the diagnosis of extracapsular extension of tumor and for detection of seminal vesicle, neurovascular bundle, and pelvic organ invasion (Claus et al. 2004). Furthermore, the zonal anatomy of the prostate is well depicted with TSE T2-weighted MR imaging. The peripheral zone appears as an area of increased T2 signal intensity (due to glandular content) which is well delineated from the central gland by the compressed central zone. Approximately 70 % of prostate cancers arise in the peripheral zone and appear as focal areas of low signal intensity foci on T2-weighted images due to decreased glandular content (Claus et al. 2004).

17.6.1 Prostate Tumor Pitfalls

Pitfall: *Not everything that is of low signal intensity on T2 weighted images in the peripheral zone is tumor*. The finding of a low T2 signal intensity focus in the peripheral zone of the prostate is actually quite nonspecific and can be attributed to other etiologies. Post-biopsy hemorrhage is a common cause of low T2 signal intensity and low T2 signal intensity foci must be correlated with T1-weighted imaging (Claus et al. 2004). Since the majority of patients are imaged with MRI for local staging after TRUS biopsy, it is not uncommon to observe post-biopsy hemorrhage in the peripheral zone. Many institutions recommend a 6–8 week interval between biopsy and MRI to allow time for the blood to be resorbed. Post-biopsy hemorrhage is usually of increased T1

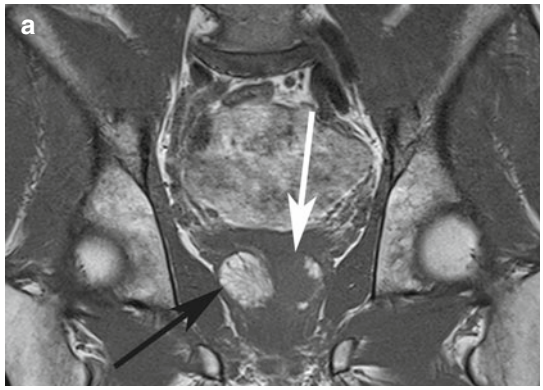

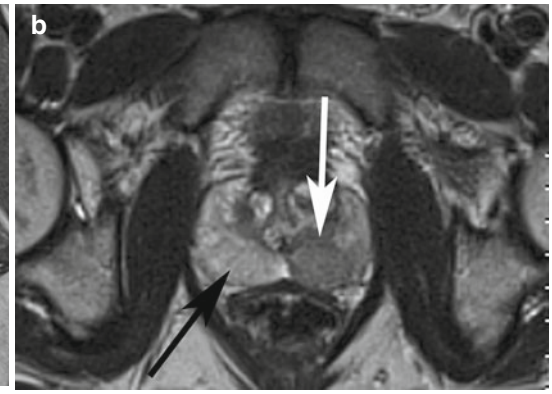

Fig. 17.17 (**a**) Coronal T1-W MR image taken 3 weeks post-prostate biopsy shows a large area of high signal intensity consistent with an area of hemorrhage (*black arrow*). The tumor (*white arrow*) is of low signal intensity. (**b**) Axial T2-W image shows that there is no bleeding within the tumor (*white arrow*). The area of hemorrhage retains its high signal (*black arrow*)

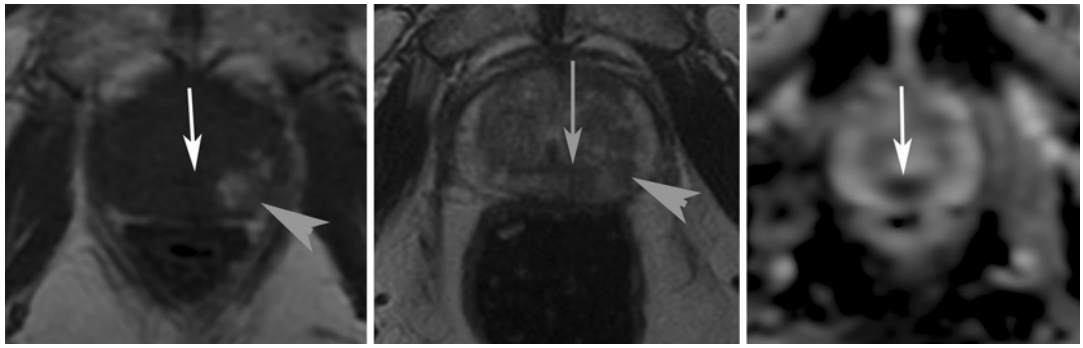

Fig. 17.18 Seventy-five-year-old man with biopsy-proven Gleason score 8 (4+4) tumor in the left medial middle peripheral zone of the prostate. (*Left*) Axial TSE T1-W and (*middle*) axial TSE T2-W MR images and (*right*) apparent diffusion coefficient (ADC) map show an area of post-biopsy hemorrhage in the left lateral peripheral zone which is of low T2 signal (*white arrowhead*). This mimics an underlying tumor. There is a lack of restricted diffusion in this location. The true tumor is seen as an area of low T2 signal intensity (*white arrow*) without corresponding increased T1 signal and low signal intensity (restricted diffusion) on the ADC map. Post-biopsy hemorrhage in the peripheral zone can mimic tumor on T2-W sequences. Axial T1-W pulse sequences must be correlated with T2-W images to confirm that areas of low T2 signal represent tumor and not hemorrhage

signal intensity and decreased T2 signal intensity (intracellular methemoglobin) and can be mistaken for tumor when using only T2-weighted sequences. Comparison of T1- and T2-weighted images in the axial plane is often of most benefit for the differentiation between tumor and hemorrhage (Claus et al. 2004) (Fig. 17.17a, b).

17.6.2 Prostate Iatrogenic Pitfalls

Post-biopsy hemorrhage can be a helpful finding when searching for a primary tumor in the peripheral zone. Decreased concentrations of citrate (a natural anticoagulant) within tumor cause the primary tumor to appear of low T1 signal intensity in relation to the increased T1 signal intensity of the hemorrhagic peripheral zone. This finding is referred to as the hemorrhage exclusion sign and has a reported specificity of 96 % for diagnosis of primary tumor, when identified in an area of homogeneous low signal intensity on T2-weighted images (Barret et al. 2012; Purysko and Herts 2012) (Fig. 17.18). Other causes of low signal intensity on T2-weighted images in the peripheral zone of the prostate gland include acute and chronic prostatitis and postradiation therapy change (Claus et al. 2004) (Fig. 17.19a, b).

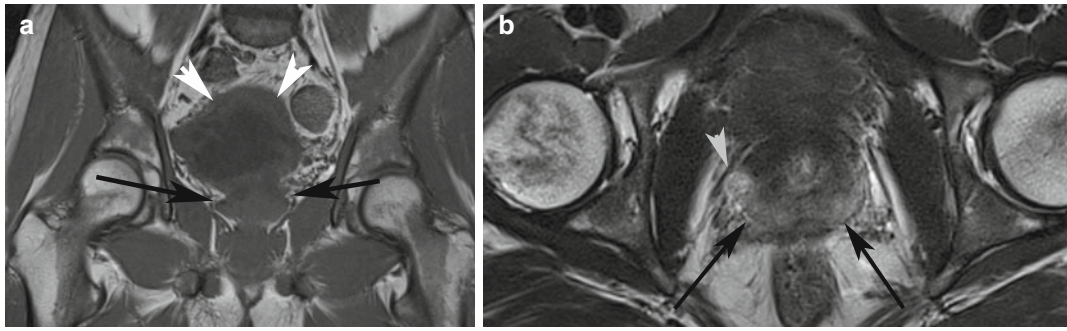

Fig. 17.19 Twenty-nine-year-old man with neurogenic bladder and chronic prostatitis (same patient as in Fig. 17.12). (**a**) Coronal T1-W MR image shows normal low signal intensity in the prostate (*black arrows*) indicating lack of hemorrhage in the tissue (patient had not undergone a biopsy). Diffuse bladder wall thickening (*white arrowheads*) related to neurogenic bladder is present. (**b**) Axial T2-W MR image shows diffuse reduced signal intensity in the peripheral zone (*black arrows*) consistent with diffuse prostatitis. There is a small area (*white arrowhead*) of residual normal/expected high signal intensity in the peripheral zone on the right side

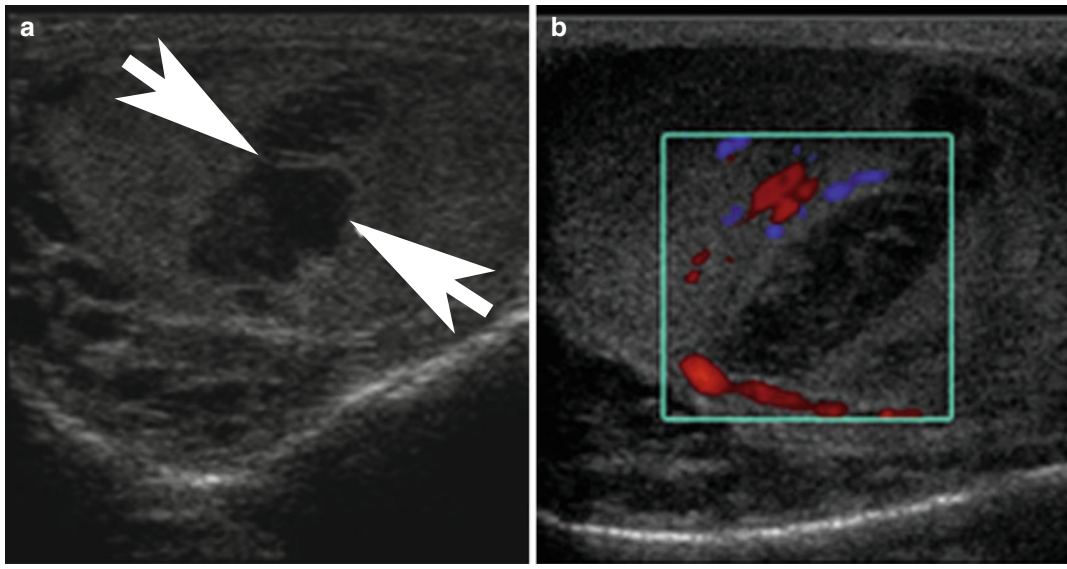

Fig. 17.20 Patient with scrotal trauma and resultant fracture. (**a**) Ultrasound image shows a well circumscribed hypoechoic area (*arrowheads*). (**b**) On the corresponding color Doppler image, there is no flow within this area, consistent with hematoma. Nevertheless, this area requires follow up to ensure that there is no underlying malignancy

17.7 Pitfalls in Imaging the Scrotum

Ultrasound imaging is the most used modality for evaluating the testicles. The benefits of ultrasound imaging include easy accessibility to ultrasound equipment, real-time imaging, dynamic imaging (in cases of hernia evaluation), and Doppler evaluation of flow. Trauma, infections, and neoplasms are common indications for imaging the scrotum and testicles. Trauma to the testicle includes intratesticular hematoma, fracture of the testicle (Fig. 17.20), and testicular rupture. Appearances of each type of injury vary with time. Blood/hematoma can be isoechoic hyperacutely. In the acute and subacute phase, the blood products are often heterogeneously hyperechoic. In the chronic phase, the areas become hypoechoic (Barret et al. 2012).

17.7.1 Scrotal Trauma Pitfalls

Pitfall: *In patients with scrotal trauma, neoplasms are present in 10–15% of patients but*

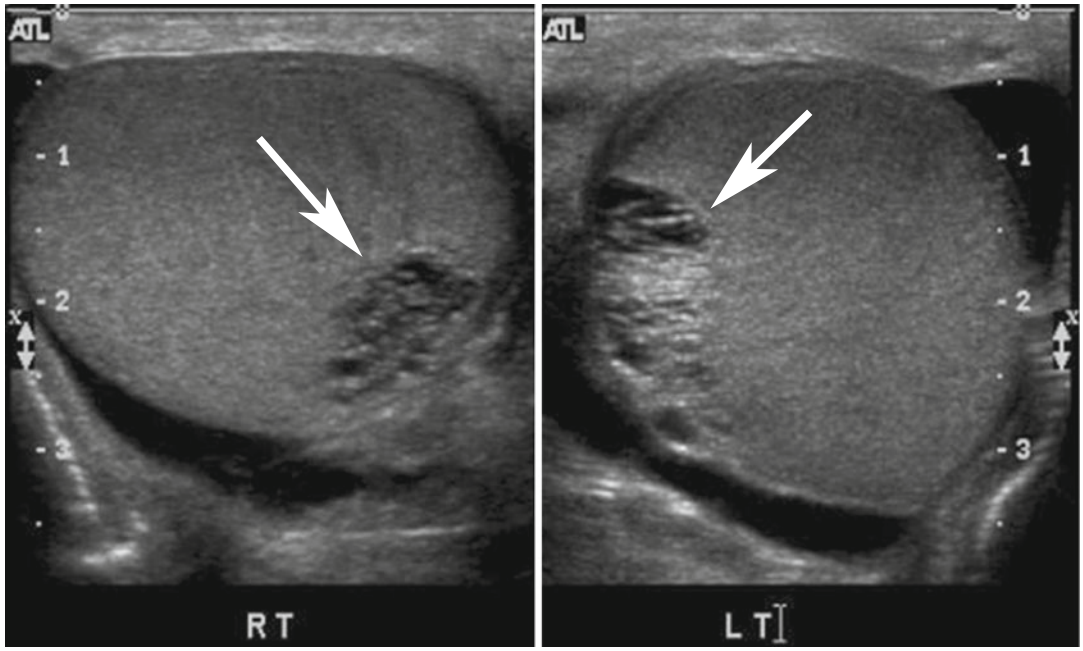

Fig. 17.21 Scrotal ultrasound images of a 68-year-old man show incidental finding of dilated rete testes bilaterally (*arrows*). These are the typical location and appearance of this benign finding

may be masked by blood. Tumors may bleed or cause pain, even with minor trauma. In addition, tumors can resemble hematomas, especially when necrotic. Thus, in any patient who is being treated conservatively for testicular hematoma (Fig. 17.20), follow-up imaging to resolution is required in order to ensure that there is no underlying mass (Bhatt and Dogra 2008; Kratzik et al. 1989). When evaluating testicles, it is important to note that there are benign intratesticular structures which can lead to false-positive diagnosis of neoplasms. This includes dilated rete testes (Fig. 17.21), a tiger stripe pattern seen in some normal testicles, as well as adrenal rests which can be rarely found in patients with congenital adrenal hyperplasia (Budzyńska and Beń-Skowronek 2011) (Fig. 17.22).

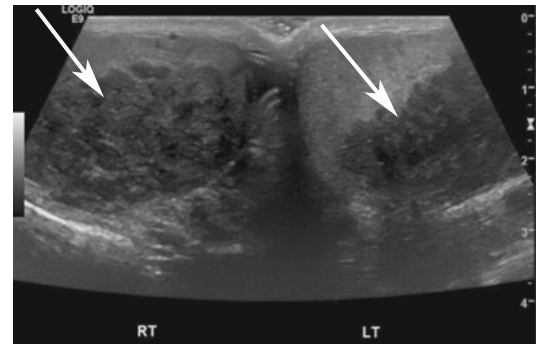

Fig. 17.22 Scrotal ultrasound images of a 21-year-old man with known congenital adrenal hyperplasia on follow-up show bilateral adrenal rests in both testicles (*arrows*). Without the clinical history, malignancy would have been the most likely diagnosis

The tunica albuginea is the strong fibrous layer that surrounds the testis; it can sustain a force of up to 50 kg before rupturing (Bhatt and Dogra 2008). Assessment of the integrity of the tunica in suspected cases of testicular rupture is challenging. Studies have confirmed that relying solely on direct visualization of a tunica defect for testicular fracture is not optimal, with sensitivity and specificity of only 50 and 76 %, respectively (Guichard et al. 2008). However, the loss of normal oval testicular contour and abnormal testicular echotexture as criteria of rupture has a much higher diagnostic accuracy, with ranges of sensitivity of 90–100 % and specificity of 65–93 % (Kim et al. 2007; Guichard et al. 2008). A diagnostic strategy that optimizes sensitivity at

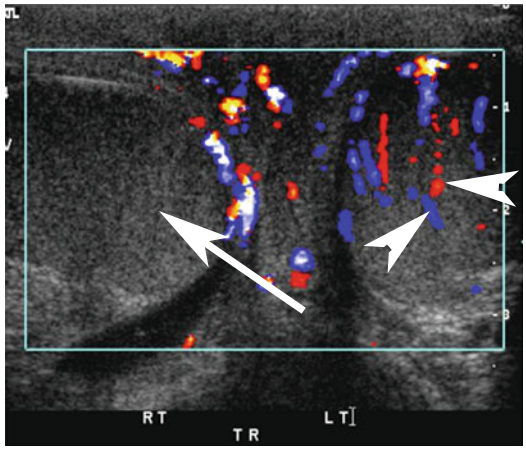

Fig. 17.23 Sixteen-year-old boy who had sudden onset of right testicular pain 10 h earlier. Doppler ultrasound images of both testicles show the lack of flow in the right testicle (*arrow*), compared to the normally vascularized left testicle (*white arrowheads*). At surgery, the right testicle was found to be non-salvageable due to torsion

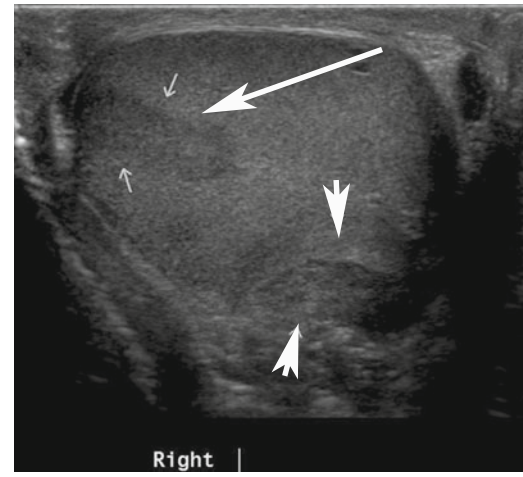

Fig. 17.24 Thirty-year-old man with sudden pain a few days ago which subsided but he returned 2 days later. Ultrasound image shows areas of reduced echogenicity in the parenchyma of the right testicle (*arrows*). The epididymis appears to be unusually positioned with respect to the testicle (*arrowheads*). There was some flow in the testicle except in the area of hypoechogenicity. At surgery, a bell-clapper deformity was identified with incomplete torsion. The hypoechoic area reduced in size over time and was felt to represent an area of focal ischemia

the expense of specificity is reasonable, since it means that few ruptures will be missed. The morbidity of missed rupture which includes orchidectomy, infection, and development of antisperm antibodies likely outweighs the morbidity of surgical exploration for a case of non-rupture. The lower specificity of ultrasound imaging for diagnosis of rupture is partly due to intratesticular hematomas which can cause abnormalities in the testicular contour without disruption of the tunica albuginea.

17.7.2 Testicular Torsion Pitfalls

Pitfall: *Arterial flow in the testicle does not exclude acute torsion*. Torsion is a urologic emergency and ultrasound imaging is the modality of choice for evaluation (Fig. 17.23). Time from torsion to treatment is the most important factor in salvage rates. A salvage rate of nearly 100 % has been described, when treated within 6 h. This drops to 20 % when treatment occurs within 12–24 h (Patriquin et al. 1993). The severity of torsion of the testis can range from 180° to 720°, but complete occlusion of arterial flow does not occur until 450° of torsion (Dogra et al. 2003). Thus, if there is only partial torsion, some arterial blood flow may still be documented, due to high systolic pressures. Despite advances in technology and operator experience, color Doppler ultrasound imaging can still result in false-negative diagnoses (Ingram et al. 1993) (Fig. 17.24). Echogenicity of the testicle can be normal early on but often decreases over ensuing hours. Providing an image with both testicles in the field of view is a key method to directly compare the testicles. This including showing variable or reduced amplitude of Doppler tracings on the affected side and compared to the normal side (Cassar et al. 2008). Reversal of diastolic flow is another important early sign to identify on Doppler tracing of the abnormal side (Dogra et al. 2003).

17.7.3 Epididymitis Pitfalls

Pitfall: *The differentiation of traumatic from infectious epididymitis is not possible by imaging*; *clinical history must be used to determine the diagnosis* (Gordon et al. 1996). Imaging appearances of these two conditions overlap. Another potential pitfall in evaluating the epididymis

can occur in patients with previous vasectomy. In these patients, almost 50 % develop changes which have characteristic appearances on ultrasound imaging. This includes general thickening, epididymal tubular ectasia, and presence of sperm granuloma (Reddy et al. 2004). However, the enlarged appearance and more prominent hypoechogenicity can be a pitfall leading to false-positive diagnosis of acute epididymitis. Obtaining a history of vasectomy and correlation with acute history is often helpful.

17.7.4 Extratesticular Masses

The vast majority of lesions in the scrotum which are not within the actual testicle parenchyma are benign (Beccia et al. 1976). Hernias should be differentiated from other solid lesions along the spermatic cord since the surgical approach varies. Lipomas are one of the most common solid lesions along the spermatic cord, followed by adenomatoid tumors which arise from the epididymis (Cassidy et al. 2010). Rarely, liposarcomas or other sarcomas can occur in this location (Dogra et al. 2003). Complacency can lead to a pitfall in imaging the scrotum; increase in size over time and presence of soft tissue and vascular components can help differentiate common lipomas from malignant counterparts.

17.7.5 Scrotal Air

Fournier gangrene is a serious infection caused by a number of different organisms, which has a predilection for patients with diabetes mellitus and other immunocompromised states. Patients often present with severe pain, significant testicular swelling, and crepitus. This aggressive, ascending infection often produces gas in the subcutaneous tissues, leading to the development of crepitus (Kube et al. 2012). On ultrasound imaging, significant soft tissue thickening and peritesticular fluid are common but nonspecific. *A pitfall of ultrasound imaging of the scrotum is the possibility of missing subcutaneous gas*. Echogenic foci with dirty shadowing and reverberation artifact should raise concerns of gas in tissues (Dogra et al. 2003). This can be confirmed with CT or radiographs (Kube et al. 2012) (Fig. 17.25a, b). A differential diagnosis to consider is air tracking from another subcutaneous source, such as from a pneumothorax, leading to subcutaneous emphysema and tracking towards the scrotum. This can be seen in trauma patients who are kept in Trendelenburg positions for extended periods of time (Fig. 17.26a–c). Patients with air in the scrotum from noninfectious causes are usually asymptomatic, other than noticing a sudden increase in size of the scrotum.

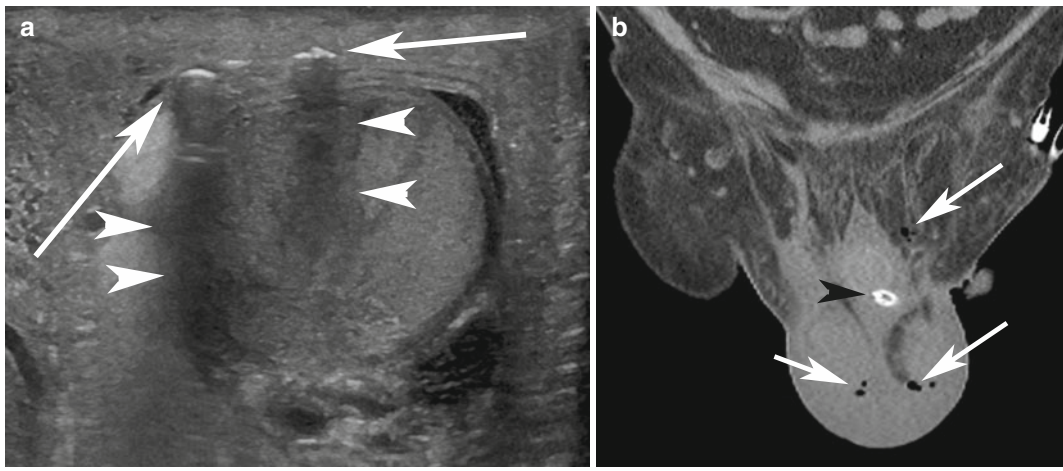

Fig. 17.25 Seventy-eight-year-old man with diabetes mellitus and diagnosis of Fournier gangrene. (**a**) Ultrasound image shows foci of air (*arrows*) in the subcutaneous tissues, identified as echogenic areas with shadowing (*arrowheads*). (**b**) Follow-up coronal CT image confirms this diagnosis of multiple air bubbles (*white arrows*). The *black arrowhead* denotes the Foley catheter

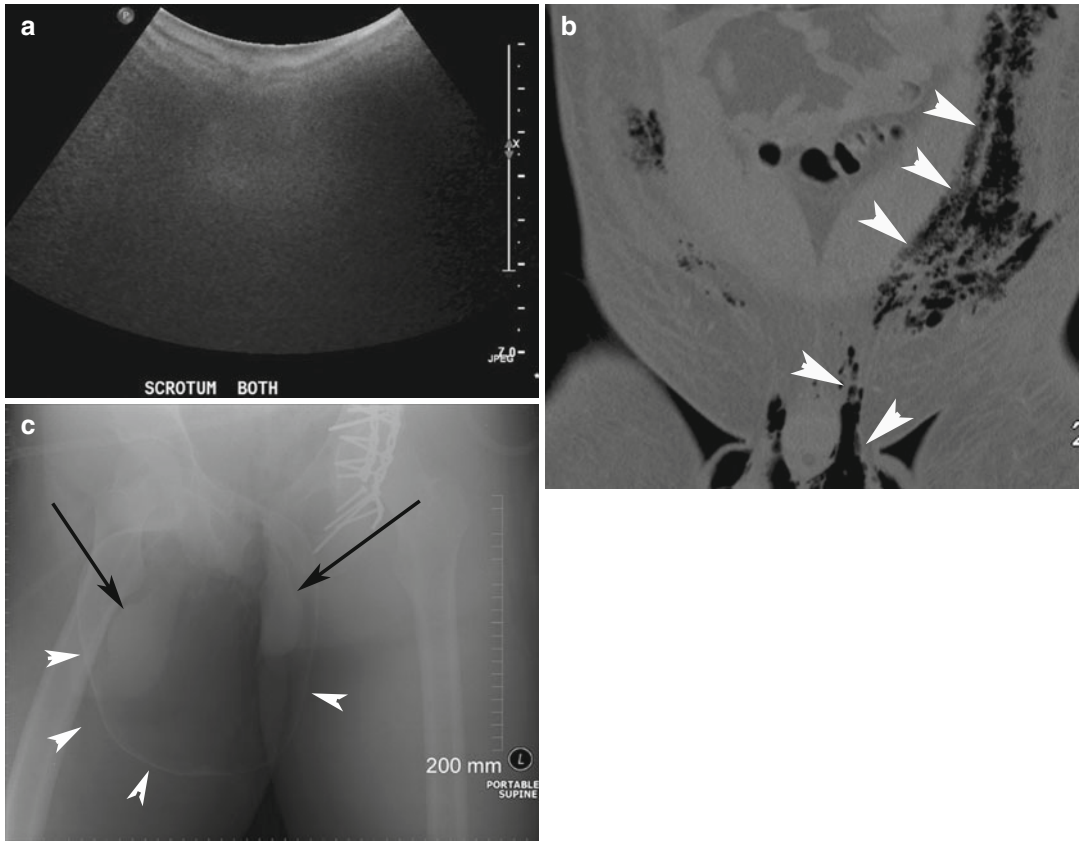

Fig. 17.26 Twenty-seven-year-old man with polytrauma 2 days previously. An acutely enlarged scrotum was noted when the patient was in the operating room for repair of a complex hip fracture. Patient had been placed in Trendelenburg position for several hours. (**a**) Ultrasound image fails to identify any normal structure in the scrotum due to presence of air. (**b**) Follow-up coronal CT image shows subcutaneous air (*arrowheads*) tracking under the skin towards the scrotum on both sides. (**c**) Radiograph of the scrotum shows a large amount of air in the scrotal sac (*white arrowheads*). The *black arrows* depict the testicles within the scrotal sac, outlined by large amounts of air

17.8 Pitfalls in Imaging the Penis

Imaging of the penis can lead to pitfalls, usually due to lack of experience, as it is not a frequently encountered request. Infection post-intervention (e.g., penile lengthening surgery) and chronic strictures from sexually transmitted diseases can lead to collections around the urethra which often communicate with it or with the skin (e.g., watering can perineum described with chronic gonorrhea) (Sharfi and Elarabi 1997). Trauma to the groin can involve tears of the penile tunica albuginea. These are commonly referred to as "penile fractures" and only occur while the penis is erect. Patients usually report hearing a "crack," in addition to a popping sensation at the time of the trauma. This is followed by pain, detumescence, swelling, and discoloration (Ramchandani and Buckler 2009). Ultrasound imaging may be requested preoperatively to identify the location and extent of the tear to the tunica albuginea and to exclude involvement of the corpora spongiosum or urethra. The defect in the tunica albuginea allows blood from the corpora cavernosa to form a hematoma in the surrounding soft tissues (Fig. 17.27). Artificial urinary sphincters can be used in treatment of stress incontinence after prostatectomy (Van der Aa et al. 2013).

Pitfall: *On ultrasound imaging*, *penile implants and artificial urinary sphincters can be misinterpreted as masses*, *if a clinical history is not provided*. These implanted structures

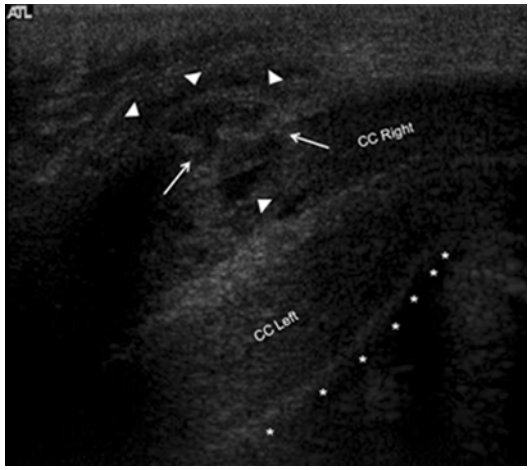

Fig. 17.27 Penile fracture. Sagittal US image taken through the base of the penis of a 41-year-old man following direct trauma to the erect penis shows a defect in the right-sided tunica albuginea (*white arrows*) and a hematoma (*white triangles*) both within and outside of the right corpus cavernosum (*CC*). The left-sided penile tunica albuginea (echogenic band just superior to the *) is normal. At surgery, the tunica albuginea defect was successfully repaired (Case courtesy of Dr. Margaret Fraser Hill)

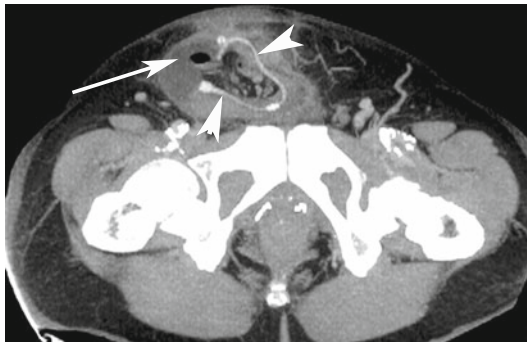

Fig. 17.28 Fifty-nine-year-old patient with artificial urethral sphincter placed post-prostatectomy for urinary incontinence. The patient presented with fever and pain 3 weeks after placement of the device. Axial CT image shows the pump and tubing in the right groin area (*white arrowheads*). There is an abscess (*arrow*) which has developed around the pump and tubing. On ultrasound imaging (not shown), this appeared as a heterogeneous mass and, without appropriate history, could not be diagnosed until CT was performed on follow-up

have a pump in the inguinal or scrotal area. In symptomatic patients, imaging may demonstrate associated with peri-implant infections or hernia (Fig. 17.28).

Conclusion

Pitfalls and potential interpretation errors in GU imaging can be avoided with experience, attention to detail, and obtaining a useful clinical history in order to use the best imaging modality and technique to answer the clinical question. Challenges remain in cases where there are similarities in imaging features. Different imaging modalities often can complement each other in making a final diagnosis.

References

Ahmad NA, Ather MH, Rees J (2003) Incidental diagnosis of diseases on un-enhanced helical computed tomography performed for ureteric colic. BMC Urol 3:2

AracM CH, Oner AY et al (2005) Distinguishing pelvic phleboliths from distal ureteral calculi: thin-slice CT findings. Eur Radiol 15:65–70

Avni EF, Bali MA, Regnault M et al (2002) MR urography in children. Eur J Radiol 43:154–166

Barrett T, Vargas HA, Akin O et al (2012) Value of the hemorrhage exclusion sign on T1-weighted prostate MR images for the detection of prostate cancer. Radiology 263:751–757

Beccia DJ, Krane RJ, Olsson CA (1976) Clinical management of non-testicular intrascrotal tumors. J Urol 116:476–479

Bhatt S, Dogra V (2008) Role of US in testicular and scrotal trauma. Radiographics 28:1617–1629

Bhatt S, MacLennan G, Dogra V (2007) Renal pseudotumors. AJR Am J Roentgenol 188:1380–1387

Blake M, Krishnamoorthy SK, Boland GW et al (2003) Low density pheochromocytoma on CT: a mimicker of adrenal adenoma. AJR Am J Roentgenol 181: 1663–1668

Blake MA, Kalra MK, Sweeney AT et al (2006) Distinguishing benign from malignant adrenal masses: multi-detector row CT protocol with 10-minute delay. Radiology 238:578–585

Boland GW, Hahn PF, Pen˜a C et al (1997) Adrenal masses: characterization with delayed contrast enhanced CT. Radiology 202:693–696

Boland GW, Lee MJ, Gazelle GS et al (1998) Characterization of adrenal masses using unenhanced CT: an analysis of the CT literature. AJR Am J Roentgenol 171:201–204

Budzyńska E, Beń-Skowronek I (2011) Testicular adrenal rest tumours in boys with congenital adrenal hyperplasia: case report and literature review. Pediatr Endocrinol Diabetes Metab 17:239–242

Caoili EM, Korobkin M, Francis IR et al (2000) Delayed enhanced CT of lipid-poor adrenal adenomas. AJR Am J Roentgenol 175:1411–1415

Caoili EM, Cohan RH, Inampudi P et al (2005) MDCT urography of upper tract urothelial neoplasms. AJR Am J Roentgenol 184:1873–1881

Cassar S, Bhatt S, Paltiel HJ, Dogra VS (2008) Role of spectral Doppler sonography in the evaluation of partial testicular torsion. J Ultrasound Med 27: 1629–1638

Cassidy FH, Ishioka KM, McMahon CJ et al (2010) MR imaging of scrotal tumors and pseudotumors. Radiographics 30:665–683

Catalona WJ, Richie JP, Ahmann FR et al (1994) Comparison of digital rectal examination and serum prostate specific antigen in the early detection of prostate cancer: results of a multicenter clinical trial of 6,630 men. J Urol 151:1283–1290

Choi YA, Chan KK, Park BK, Kim B (2013) Evaluation of adrenal metastases from renal cell carcinoma and hepatocellular carcinoma: use of delayed contrast enhanced CT. Radiology 266:514–520

Chu PL, Wei YF, Huang J et al (2006) Clinical characteristics of patients with segmental renal infarction. Nephrology (Carlton) 11:336–340

Claus F, Hricak H, Hattery RR (2004) Pretreatment evaluation of prostate cancer: role of MR imaging and 1H MR spectroscopy. Radiographics 24:S167–S180

Colistro R, Torreggiani WC, Lyburn ID et al (2002) Unenhanced helical CT in the investigation of acute flank pain. Clin Radiol 57:435–441

Corriere JN Jr, Sandler CM (1986) Management of the ruptured bladder: seven years of experience with 111 cases. J Trauma 26:830–833

D'Angelo PC, Gash JR, Horn AW, Klein FA (2002) Fat in renal cell carcinoma that lacks associated calcifications. AJR Am J Roentgenol 178:931–932

Delfaut EM, Beltran J, Johnson G et al (1999) Fat suppression in MR imaging: techniques and pitfalls. Radiographics 19:373–382

Dogra VS, Gottlieb RH, Oka M, Rubens DJ (2003) Sonography of the scrotum. Radiology 227:18–36

Elsayes KM, Mukundun G, Narra VR et al (2004) Adrenal masses: MR imaging features with pathologic correlation. Radiographics 24:S73–S86

Farrelly C, Delaney H, McDermott R, Malone D (2008) Do all non-calcified echogenic renal lesions found on ultrasound need further evaluation with CT? Abdom Imaging 33:44–47

Garin JM, Marco I, Salva A et al (2007) CT and MRI in fat containing papillary renal cell carcinoma. Br J Radiol 80:e193–e195

Glazer HS, Weyman PJ, Sagel SS et al (1982) Nonfunctioning adrenal masses: incidental discovery on computed tomography. AJR Am J Roentgenol 139: 81–85

Gokan T, Ohgiya Y, Nobusawa H, Munechika H (2005) Br J Radiol 78:170–174

Gordon LM, Stein SM, Ralls PW (1996) Traumatic epididymitis: evaluation with color Doppler sonography. AJR Am J Roentgenol 166:1323–1325

Grattan-Smith JD, Jones RA (2006) MR urography in children. Pediatr Radiol 36:1119–1132

Guichard G, El Ammari J, Del Coro C et al (2008) Accuracy of ultrasonography in diagnosis of testicular rupture after blunt scrotal trauma. Urology 71:52–56

Haider MA, Ghai S, Jhaveri K et al (2004) Chemical shift MR imaging of hyperattenuating (>10 HU) adrenal masses: does it still have a role? Radiology 231: 711–716

Heneghan JP, Dalrymple NC, Verga M et al (1997) Soft-tissue "rim" sign in the diagnosis of ureteral calculi with use of unenhanced helical CT. Radiology 202:709–711

Hindman N, Ngo L, Genega EM et al (2012) Angiomyolipoma with minimal fat: can it be differentiated from clear cell renal cell carcinoma by using standard MR techniques. Radiology 265:468–477

Ingram S, Hollman AS, Azmy A (1993) Testicular torsion: missed diagnosis on color Doppler sonography. Pediatr Radiol 23:483–484

Israel GM, Bosniak MA (2008) Pitfalls in renal mass evaluation and how to avoid them. Radiographics 28:1325–1338

Jin DH, Lamberton GR, Broome DR et al (2009) Renal stone detection using unenhanced multidetector row computerized tomography–does section width matter? J Urol 181:2767–2773

Johnson PT, Horton KM, Fishman EK (2009) Adrenal imaging with multidetector CT: evidence-based protocol optimization and interpretative practice. Radiographics 29:1319–1331

Kane AJ, Wang ZJ, Qayyum A et al (2012) Frequency and etiology of unexplained bilateral hydronephrosis in patients with breast cancer: results of a longitudinal CT study. Clin Imaging 36:263–266

Khan AN, Lin EC (2013) Transitional cell carcinoma imaging. Medscape references. http://emedicine.medscape.com/article/381323-overview Accessed 15 Jan 2013

Kielar AZ, McInnes M, Quon M et al (2011) Introduction of QUIP (quality information program) as a semi-automated quality assessment endeavor allowing retrospective review of errors in cross-sectional abdominal imaging. Acad Radiol 18:1358–1364

Kielar AZ, Shabana W, Vakili M, Rubin J (2012) Prospective evaluation of Doppler sonography to detect the twinkling artifact versus unenhanced computed tomography for identifying urinary tract calculi. J Ultrasound Med 3:1619–1625

Kim JC (2001) Central lucency of pelvic phleboliths: comparison of radiographs and non contrast helical CT. Clin Imaging 25:122–125

Kim BS, Hwang IK, Choi Y et al (2005) Low-dose and standard-dose unenhanced helical computed tomography for the assessment of acute renal colic: prospective comparative study. Acta Radiol 46:756–763

Kim JK, Kim SH, Jang YJ et al (2006) Renal angiomyolipoma with minimal fat: differentiation from other neoplasms at double-echo chemical shift FLASH MR imaging. Radiology 239:174–180

Kim SH, Park S, Choi SH et al (2007) Significant predictors for determination of testicular rupture on sonography. J Ultrasound Med 26:1649–1655

Korobkin M, Brodeur FJ, Francis IR et al (1998) CT time attenuation washout curves of adrenal adenomas and nonadenomas. AJR Am J Roentgenol 170:747–752

Kratzik CH, Hainz A, Kuber W et al (1989) Has ultrasound influenced the therapy concept of blunt scrotal trauma? J Urol 142:1243–1245

Kube E, Stawicki SP, Bahner DP (2012) Ultrasound in the diagnosis of Fournier's gangrene. Int J Crit Ill Inj Sci 2:104–106

Lawrentschuk N, Fleshner N (2009) The role of magnetic resonance imaging in targeting prostate cancer in patients with previous negative biopsies and elevated prostate-specific antigen levels. BJU Int 103:730–733

Lee MJ, Hahn PF, Papanicolaou N et al (1991) Benign and malignant adrenal masses: CT distinction with attenuation coefficients, size, and observer analysis. Radiology 179:415–418

Levine D, Filly RA (1994) Using color Doppler jets to differentiate a pelvic cyst from a bladder diverticulum. J Ultrasound Med 13:575–577

Marhuenda A, Martín MI, Deltoro C et al (2008) Radiologic evaluation of small renal masses (I): pretreatment management. Adv Urol 2008:1–16, Article ID 415848

Maynor CH, Kliewer MA, Hertzberg BS et al (1996) Urinary bladder diverticula: sonographic diagnosis and interpretive pitfalls. J Ultrasound Med 15:189–194

Merran S, Vieillefond A, Peyromaure M, Dupuy C (2004) Renal angiomyolipoma with calcification: CT-pathology correlation. Br J Radiol 77:782–783

Mitchell DG, Crovello M, Matteucci T, Petersen RO, Miettinen MM (1992) Benign adrenocortical masses: diagnosis with chemical shift MR imaging. Radiology 185:345–351

Muraoka N, Sakai T, Kimura H et al (2008) Rare causes of hematuria associated with various vascular disease involving the upper urinary tract. Radiographics 28:855–867

Patriquin HB, Yazbeck S, Trinh B et al (1993) Testicular torsion in infants and children: diagnosis with Doppler sonography. Radiology 188:781–785

Pitts, ST, Niska RW, Xu J, Burt CW (2008) National Health Statistic Report. National Hospital Ambulatory Medical Care Survey: 2006 Emergency Department Summary

Purysko AS, Herts BR (2012) Prostate MRI: the hemorrhage exclusion sign. J Urol 188:1946–1947

Rahmouni A, Bargoin R, Herment A et al (1996) Color Doppler twinkling artifact in hyperechoic regions. Radiology 199:269–271

Ramchandi P, Buckler PM (2009) Imaging of genitourinary trauma. AJR Am J Roentgenol 192:1514–1523

Reddy NM, Gerscovich EO, Jain KA et al (2004) Vasectomy-related changes on sonographic examination of the scrotum. J Clin Ultrasound 32:394–398

Sahdev A, Willatt J, Fracis IR, Reznek RH (2010) The indeterminate adrenal lesion. Cancer Imaging 10:102–113

Sasiwimonphan K, Takahashi M, Leibovich B et al (2012) Small (<4 cm) renal mass: differentiation of angiomyolipoma without visible fat from renal cell carcinoma utilizing MR imaging. Radiology 263:160–168

Schwartz LH, Macari M, Huvos AG, Panicek DM (1996) Collision tumors of the adrenal gland: demonstration and characterization at MR imaging. Radiology 201:757–760

Sharfi AR, Elarabi YE (1997) The 'watering-can' perineum: presentation and management. Br J Urol 80:933–936

Shinozaki K, Yoshimitsu K, Honda H et al (2001) Metastatic adrenal tumor from clear-cell renal cell carcinoma: a pitfall of chemical shift MR imaging. Abdom Imaging 26:439–442

Siegelman ES (2012) Adrenal MRI: techniques and clinical applications. J Magn Reson Imaging 36:272–285

Silverman SG, Leyendecker JR, Smis ES (2009) What is the current role of CT urography and MR urography in the evaluation of the urinary tract? Radiology 250:309–323

Song JH, Chaudhry FS, May-Smith WW (2008) The incidental adrenal mass on CT: prevalence of adrenal disease in 1049 consecutive adrenal masses in patients with no known malignancy. AJR Am J Roentgenol 190:1163–1168

Sydow B, Rosen MA, Siegelman ES (2006) Intracellular lipid within metastatic hepatocellular carcinoma of the adrenal gland: a potential diagnostic pitfall of chemical shift imaging of the adrenal gland. AJR Am J Roentgenol 187:W550–W551

Taffel M, Haji-Momenian S, Nikolaidis P, Miller FH (2012) Adrenal imaging: a comprehensive review. Radiol Clin North Am 50:219–243

Tsai CH, Yank FJ, Huang CC, Kuo CC, Chen YM (2012) Bubbles in the urinary bladder. Neth J Med 70:42–47

Tsuji T, Ohtake T, Yonemura K et al (2007) Chronic pyelonephritis presenting as multiple tumor-like renal lesions. Intern Med 46:879–882

Vaccaro JP, Brody JM (2000) CT cystography in the evaluation of major bladder trauma. Radiographics 20(5): 1373–1381

Van der Aa F, Drake MJ, Kasyan GR et al (2013) The artificial urinary sphincter after a quarter of a century: a critical systematic review of its use in male non-neurogenic incontinence. Eur Urol 63:681–689

Yoshimitsu K, Honda H, Koroiwa T et al (1999) MR detection of cytoplasmic fat in clear cell renal cell carcinoma using chemical shift gradient echo imaging. J Magn Reson Imaging 9:579–585

Zinn HL, Becker JA (1997) Peripelvic cysts simulating hydronephrosis. Abdom Imaging 22:346–347